The Cryosphere, 20, 1001–1023, 2026
https://doi.org/10.5194/tc-20-1001-2026

The Cryosphere Open Access EGU

Forest disturbances and their impact on ground surface temperatures in permafrost-underlain forest in central Mongolia

Robin B. Zweigel[1,2], Dashtseren Avirmed[3,4], Khurelbaatar Temuujin[3], Clare Webster[1,5], Hanna Lee[6], and Sebastian Westermann[1,2]

[1]Department of Geosciences, University of Oslo, Oslo, 0371, Norway
[2]Centre for Biogeochemistry in the Anthropocene, University of Oslo, Oslo, 0371, Norway
[3]Institute of Geography and Geoecology, Mongolian Academy of Sciences, Ulaanbaatar, 15170, Mongolia
[4]UNESCO Chair of Environmental Sciences in Eastern Central Asia,
Mongolian Academy of Sciences, Ulaanbaatar, 15170, Mongolia
[5]Department of Geography, University of Zurich, 8057 Zürich, Switzerland
[6]Department of Biology, Norwegian University of Science and Technology, Trondheim, 7419, Norway

Correspondence: Robin B. Zweigel (robinbz@uio.no)

Received: 20 May 2025 – Discussion started: 27 June 2025
Revised: 28 December 2025 – Accepted: 30 December 2025 – Published: 11 February 2026

Abstract. In the forest-steppe ecotone in central Mongolia, forest and permafrost exist close to their climatic limits and are co-located on north-facing slopes. The deciduous forest ecosystems and permafrost on these slopes are linked through interactions in the local energy and water balance. Furthermore, in this region the presence of such permafrost-forest systems provides essential services that supports local livelihoods and ecosystem function. However, forest disturbances that reduce or remove the forest canopies and lead to changes in surface cover could impact ground surface temperatures (GSTs) and potentially lead to permafrost degradation. In this study, we investigate the relationship between different forest states and GSTs at a site in the forest-steppe ecotone. We measured GSTs and surveyed vegetation density and surface cover over two years in an area that features both intact, dead and logged forest and dense stands of young regrowth. Overall, we find GSTs in summer and winter to vary substantially among the forest states, while differences in GST in spring and fall are small. Compared to the intact forest, the annual GST range is increased in the dead and logged forest while it is dampened in stands of young regrowth. Contrary to existing literature, we do not observe a general warming of the ground surface at disturbed sites, but instead find mean annual GSTs at disturbed sites to be 0.5 °C lower than at intact sites. We also find substantial floor vegetation in the dead and logged forest, which has implications for livestock grazing patterns and remote sensing of forest disturbances.

1 Introduction

Forest ecosystems regulate the energy and water balance of the ground below through process such as canopy shading, transpiration and accumulation of surface organic layers (Bonan and Shugart, 1989; Chasmer et al., 2011). As forest cover generally lowers ground temperatures and limits seasonal thaw depth, it provides the necessary conditions for permafrost persistence in many regions (Chang et al., 2015; Fisher et al., 2016). Disturbances to the forest cover impact its structure and function, which has implications for the ground hydrological- and thermal regime, and potentially can impact permafrost stability (Stuenzi et al., 2021b, 2022). Such disturbances to the forest cover can be biotic, for example insect infestations or diseases, or abiotic like wildfires, logging or windthrow, and we referred to them collectively as "forest disturbances". Previous work from sites affected by wildfire report reduced canopy shading, removal of surface organic layers and lower surface albedo, which enhances absorption of solar radiation and gives higher ground surface temperatures (GSTs) (Klinge et al., 2021; Kopp et al., 2014; Li et al., 2021; Yoshikawa et al., 2002). Furthermore, the re-

duction in evapotranspiration following logging is found to elevate soil moisture levels, which in turn increases active layer thickness and GSTs (Fedorov et al., 2017; Iwahana et al., 2005). However, most studies on forest disturbances in discontinuous permafrost in Mongolia focus on summer conditions (Klinge et al., 2021; Kopp et al., 2014), while year-round studies are limited to flat areas or overall different climates (Fedorov et al., 2017; Yoshikawa et al., 2002). For this reason, the impact of forest disturbances on the seasonal and annual ground temperatures at sites where hydrological and thermal conditions are strongly influenced by local terrain remains unclear.

The forest-steppe ecotone in central Mongolia is at the southern border of both the Eurasian permafrost and boreal forest regions, where deciduous forests and permafrost is primarily found on north-facing slopes and their presences are intimately linked (Dashtseren et al., 2014; Ishikawa et al., 2018; Temuujin et al., 2024). Previous research suggests that forests cover in this region lowers ground temperatures and limits active layer depths, which promote permafrost presence. The existence of a shallow permafrost table in turn elevates soil moisture levels, which are essential for the survival of forests (Klinge et al., 2021; Lange et al., 2015). The forested and permafrost underlain north-facing slopes are also important for local livelihoods and ecosystem function, as they provide essential wood, rangeland and water resources (Iijima et al., 2012; Karthe et al., 2013; Lkhagvadorj et al., 2013b, a). While the intertwined nature of permafrost-forest systems is widely documented (Dashtseren et al., 2014; Ishikawa et al., 2018; Temuujin et al., 2024; Undrakhbayar et al., 2024), their vulnerability to disturbances has received only little attention (Klinge et al., 2021). To this day, there is only sparse data on how forest disturbances in the forest-steppe ecotone affect vegetation and surface conditions and associated GSTs.

Ground surface temperature measurements are an increasingly valuable tool for research into permafrost dynamics. Unlike traditional permafrost borehole data, the acquisition of GST measurements is rather inexpensive and logistically simple, which facilitates spatially distributed observation of ground thermal dynamics. As GSTs are sampled at or near the ground surface, they include the impact of snow or vegetation layers, as well as any effects of variations in solar radiation caused by local terrain (e.g. Temuujin et al., 2024). Moreover, GST measurement can reveal dynamic changes in permafrost conditions as they respond quickly to shifts in climatic conditions or land use. While GSTs cannot directly reveal the presence or stability of permafrost, mean annual GSTs (MAGSTs) are linked to deeper ground temperatures through the thermal offset. Due to the generally higher thermal conductivity of frozen than thawed soil, the thermal offset is typically negative, which means permafrost can be expected also for somewhat positive MAGSTs (Smith and Riseborough, 2002). Moreover, GST measurements provide important validation for permafrost modelling efforts (e.g. Schmidt et al., 2021; Zweigel et al., 2021, 2024a).

In this study, we investigate forest disturbances and their effect on vegetation structure and density, surface cover and GSTs in Mongolia. We measure GSTs for 2 years and survey vegetation and surface cover in a study area in central Mongolia where different forest disturbance states (intact, dead, logged and young regrowth) occur at sites with similar topographic characteristics. Based on these observations, we seek to answer the following questions:

1. What are the effects of forest disturbances on vegetation densities in the canopy and forest floor, surface organic layers and snow cover?

2. How are annual and seasonal GSTs impacted by changes in forest and surface cover associated with forest disturbance?

2 Study area and methods

2.1 Site description

We collected field data over a period of 25 months at sites in the Bayanzurkh mountains in central Mongolia. Our study area (ca. 47.83° N, 107.22° E) is located in the forest-steppe ecotone in the southern part of the Khentii mountain range, 20 km east of Mongolia's capital Ulaanbaatar (Fig. 1b). This region of Mongolia is located at the southern margin of the Eurasian permafrost extent, with a transition in the study area from continuous permafrost in high-elevation areas in the northeast to sporadic permafrost in lower lying areas in the southwest. The study area is located in the discontinuous permafrost zone (Fig. 1b), where permafrost and forest cover are co-located on north-facing slopes, while south-facing slopes feature permafrost-free steppe (Temuujin et al., 2024). Climatic, permafrost and subsurface conditions have been studied for two decades around the Terelj station (Fig. 1b), which features similar topographic, climatic and vegetation characteristics as our study area (Dashtseren et al., 2014; Ishikawa et al., 2005; Temuujin et al., 2024). Here, borehole data below a mature larch forest shows wintertime and summertime GSTs of -9.4 to -11.2 and 9.0 to 10.2 °C, respectively, and permafrost with an active layer of 2.4–2.7 m (Dashtseren et al., 2014). Furthermore, Temuujin et al. (2024) studied the relationship between topographic characteristics, vegetation cover and GSTs in Terelj using spatially distributed measurements and found lower MAGSTs (-1 to 1 °C) below forest and on sites with limited available solar radiation. Soil composition in Terelj is described as complex, consisting of a 20–40 cm surface organic layer underlain by sand and gravel on north-facing forest sites (Ishikawa et al., 2005). Floor vegetation below the forest consists mostly of *Equisetum pretense* and *Fragaria orientalis*, while grassland sites are dominated by *Artemisia frigida*, *Potentilla acaulis*, *Agropyron cristatum*

and *Carex duriuscula* (Dashtseren et al., 2014). Snow cover below the larch forest in Terelj typically last for 140–170 d with a maximum thickness of 5–20 cm in March (Dashtseren et al., 2014; Zweigel et al., 2024a).

The climate of the study region is highly continental, with large annual amplitude in temperature and overall low precipitation (Dalai et al., 2019). Annual air temperatures and accumulated precipitation is available for the period 2000 to 2024 from a weather station in Nalaikh (Fig. 1b), located 7.5 km southeast of the study area at 1450 m a.s.l. Here, Mean Annual Air Temperatures (MAATs) ranges from −5.1 to −2.0 °C with an average of −3.3 °C, while annual precipitation ranged from 241 to 549 mm with an average of 341 mm (Fig. 2). Both MAAT and precipitation have increased over this period, with the warmest and wettest years found mostly towards the end of the period. Similar MAATs and (liquid) precipitation amounts are reported at the Terelj site (1662 m a.s.l.) that has a more similar elevation as the study area, ranging from −3.3 to −1.7 °C and 223 to 295 mm, respectively. However, both Nalaikh and Terelj are located in valley floors, and the temperature records are likely affected by the strong and frequent temperature inversions that persist during wintertime in Mongolia (Gerelchuluun and Ahn, 2014).

Semi-nomadic pastoralism is widespread in Mongolia, and several herder families use the Bayanzurkh mountains as pasture for their livestock. The spatial and temporal use of rangeland in the forest-steppe ecotone in Mongolia is described by Lkhagvadorj et al. (2013b, a): Generally, grasslands in river valleys and mountain slopes serve as the main grazing pastures, but forest edges are used in fall and at times when feed in the steppe is limited due to drought (Lkhagvadorj et al., 2013b). Livestock are traditionally kept from the forest interior so the herders can maintain an overview and to avoid the risk of insect harassment and predation by wild animals. However, there has been a substantial increase in the number of livestock since the early 1990s, and forest are increasingly used as rangeland especially by horses in winter (Lkhagvadorj et al., 2013a). Moreover, forest grazing by goats can substantially damage tree saplings (Lkhagvadorj et al., 2013b), which can limit forest regeneration and succession. Around the study area in Bayanzurkh, there are several seasonal herder camps on south-facing slopes and valley bottoms, with the closest campsite 700 m south of the ridge (Fig. 1a). Animal and car tracks from the south-facing slope suggest that at least the upper parts of the study area are used by local herder families for grazing and wood collection.

Our study area extends over three roughly parallel, northeast facing valleys that feature forest at different states of disturbance (Fig. 1). The upper parts of the western valley are covered with mature and intact forest dominated by larch (*Larix sibirica*), the most common forest tree in Mongolia (Dulamsuren et al., 2010). In the other parts of the study area, most trees have been killed by some disturbance and the dead tree trunks remain standing (Fig. 4b). Landsat imagery reveals that the forest dieback occurred between August 2000 and August 2001 (Fig. 3). While the exact type of disturbance is unclear, there are no visible signs of windthrow and burning, so biotic causes such as insect infestations or diseases seem likely. In parts of the disturbed area there is regrowth of various young deciduous trees (larch, birch and aspen), especially in the north-facing part of the central valley (Fig. 4b), as well as some highly local, dense forest stands in topographic concavities (Fig. 1). In both the intact and disturbed forests the vegetation consists of a canopy layer that is made up of intact, dead and young trees, and floor vegetation consisting mostly of grasses and dwarf shrubs. In the study area, we did not observe any surface features or landforms that are indicative of permafrost degradation. The upper ridge of the central and eastern valleys is accessible by car from the south, and the forest has largely been logged circa 150 m downslope of the ridge (Fig. 4a and c).

Within the study area we select 10 sites targeting the four distinct forest states found in the study area: intact forest, dead forest, logged forest and stands of young regrowth (Tables 1 and A1). The field sites are chosen to have broadly similar topographic characteristics (Table 1) and to avoid transitional areas between the forest states. INTACT_1 and INTACT_2 are in the intact forest in the upper part of the western valley. While the forest at both INTACT_1 and INTACT_2 forms a canopy without larger gaps, we note scattered logging and a lack of young trees at these sites. DEAD_1, DEAD_2 and DEAD_3 are in the dead forest with standing tree trunks in the lower parts of the western and central valleys (Fig. 1), where the forest floor in summer is covered by abundant grass vegetation (Fig. 4b). In the surroundings of DEAD_3, there is also some scattered, young regrowth of birch and larch. YOUNG_1 and YOUNG_2 are situated in dense stands of young aspen and larch, respectively. These stands are only 20–30 m in diameter and thus represent highly local conditions that are in stark contrast to that of the neighbouring dead forest at DEAD_2 and DEAD_3. To emphasize their small spatial extent, the young regrowth is referred to as "stands" rather than "forest". LOGGED_1, LOGGED_2 and LOGGED_3 are in the logged forest in the upper part of the central and eastern valleys (Fig. 1a). While LOGGED_1 and LOGGED_3 only feature grass vegetation, there are also scattered shrubs at LOGGED_2 (Fig. 3c). In addition to these field sites we measure air temperatures in a relatively flat area near the ridge between the western and central valley at 1810 m a.s.l. (Fig. 1a).

2.2 Temperature measurements

We measure temperatures using iButton (© Maxim) temperature loggers that we install at the field sites in summer 2022. We use iButtons of the type "DS1922L", which feature an operating range from −40 to +85 °C, and a numerical resolution and accuracy of 0.0625 and 0.5 °C, respectively (Maxim Integrated, 2015). These loggers are small

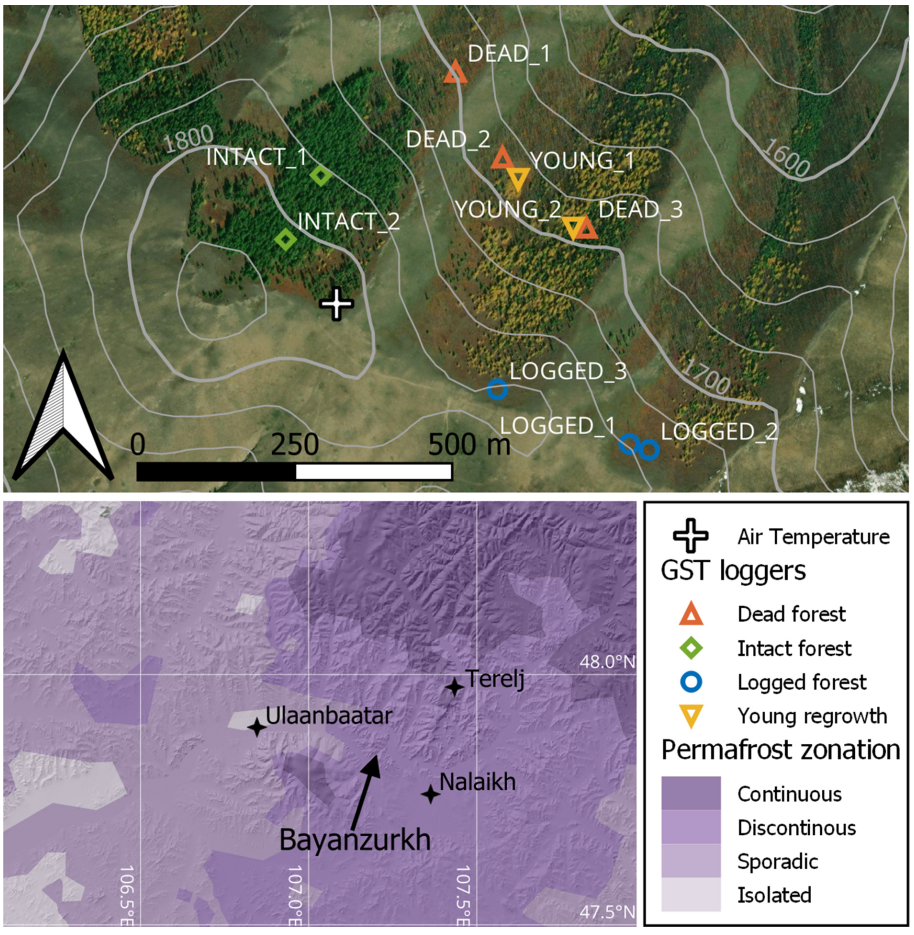

Figure 1. Overview maps of the study area. **(a)** Shows the main landcover and topographic characteristics of the study area in the Bayanzurkh mountains, as well as the location of the GST loggers and the air temperature measurement. The coloured markers for the field sites (GST loggers) are grouped by forest states. Background imagery from 10 September 2022 (Esri, 2022 | Powered by Esri) and contour lines (100 and 25 m) derived from the SRTM 30 m Digital Elevation Model (NASA JPL, 2013). **(b)** Location of the study area and places mentioned in the text within the Ulaanbaatar area, showing the permafrost zonation by Obu et al. (2019) overlaid a hillshade of the terrain (NASA JPL, 2013).

and are placed below any layers of surface organics (litter and/or moss) to measure near-surface ground surface temperature (GST). Similar setups using iButton loggers to measure GSTs have successfully been conducted at grassland- (Zweigel et al., 2024b), rockwall- (Schmidt et al., 2021) and high-arctic sites (Zweigel et al., 2021). The loggers are set to record at 4-hourly intervals, from which we compute the daily temperatures used in this study. For all sites we successfully obtain a complete 25-month record of daily temperature spanning from 10 August 2022 to 19 September 2024. Throughout this study we calculate temperature indices over the hydrological year starting on 1 September and ending on 31 August, meaning that the full hydrological years 2023 and 2024 are contained in the GST records. Note that unless specified otherwise, the GSTs and temperature-based indices presented in this study are average values for all loggers within the different forest states.

From the daily temperature records we derive temporal mean GSTs and various temperature-based indices. The mean annual GST, MAGST, is calculated over the hydrological years 2023 and 2024, while seasonal GSTs are calculated over 3-month periods for fall, winter, spring and summer (SON: September, October and November; DJF: December, January and February; MAM: March, April and May; JJA: June, July and August, respectively). In addition to average GSTs, we use the measured air temperatures and GSTs to calculate the surface offset (SO) and the scale factors for freezing (n_f) and thawing (n_t). The surface offset is given as the difference between the mean annual temperatures of the ground surface and the air (Smith and Riseborough, 2002):

$$\mathrm{SO} = \mathrm{MAGST} - \mathrm{MAAT} \quad (1)$$

Where MAAT is the mean annual air temperature over the same hydrological year as MAGST. A positive SO indicates

Table 1. Topographic characteristics for the field sites derived from the SRTM 30 m Digital Elevation Model (NASA JPL, 2013). Aspect is in degrees counterclockwise from south following the notation by Dozier and Frew (1990) and the cardinal/ordinal direction is indicated in brackets. SVF denotes the sky view fraction, i.e. the fraction of the upward facing hemisphere not obstructed by terrain. S_{in} is the average annual or seasonal incoming solar radiation in the hydrological year 2023 (September through August) using ERA5 reanalysis data (Hersbach et al., 2020) interpolated to the logger locations (Table A1) and adjusted for local terrain following Zweigel et al. (2024a). Winter and summer values are averaged over the period December–February and June–August, respectively.

Field site	Elevation [m a.s.l.]	Slope [°]	Aspect [°]	SVF [–]	S_{in} [W m^{-2}]	S_{in} [W m^{-2}] (winter)	S_{in} [W m^{-2}] (summer)
INTACT_1	1778	14.7	141 (NE)	0.95	143	78	159
INTACT_2	1808	17	138 (NE)	0.95	146	82	162
DEAD_1	1690	18.7	117 (NE)	0.94	144	83	160
DEAD_2	1686	17.1	128 (NE)	0.94	141	78	158
DEAD_3	1690	18.9	172 (N)	0.94	127	60	145
YOUNG_1	1686	17.9	128 (NE)	0.94	141	78	157
YOUNG_2	1692	19.3	167 (N)	0.94	126	60	144
LOGGED_1	1748	14.8	131 (NE)	0.95	146	82	162
LOGGED_2	1742	15.8	131 (NE)	0.95	144	80	160
LOGGED_3	1775	8.1	187 (N)	0.96	156	92	171

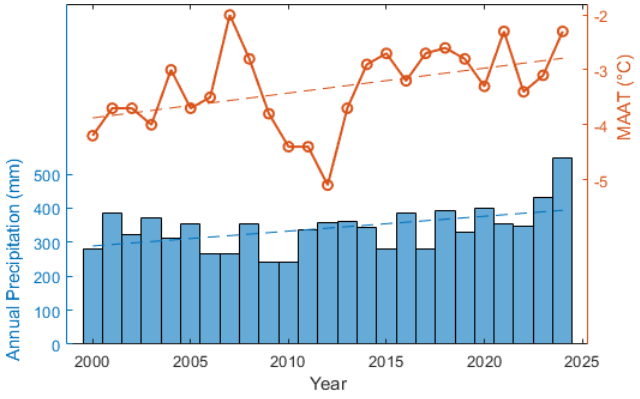

Figure 2. Climatic conditions at the Nalaikh station from 2000 to 2024. Orange line: Mean annual air temperature. Blue bars: Annual precipitation. Dashed lines show the corresponding trends over the period, which are 0.05 °C yr^{-1} and 4.4 mm yr^{-1}.

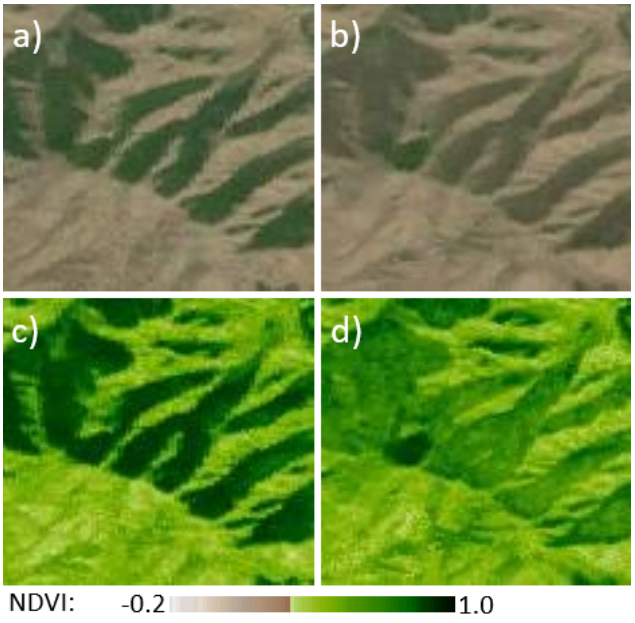

Figure 3. Remotely sensed evidence of forest disturbance in Bayanzurkh. **(a)** and **(c)** show RGB and NDVI imagery, respectively, from August 2000, while **(b)** and **(d)** show corresponding imagery from August 2001. Imagery from the 30 m Landsat-derived GWELDMO product (Version 3.1) (Roy and Zhang, 2019).

that on annual scales, processes related snow and vegetation cover give higher ground surface temperatures than air temperatures. The scale factors for freezing and thawing are calculated following (Smith and Riseborough, 1996):

$$n_f = \frac{FDD_{air}}{FDD_{surface}} \quad (2)$$

$$n_t = \frac{TDD_{air}}{TDD_{surface}} \quad (3)$$

Where FDD and TDD denote the freezing and thawing degree days defined as:

$$FDD = \sum_{i=1}^{n} |T_i|, \; T_i < 0\,°C \quad (4)$$

$$TDD = \sum_{i=1}^{n} |T_i|, \; T_i > 0\,°C \quad (5)$$

Here, T_i is the daily averaged temperature of the air or ground surface, and n is the number of days per hydrological year. n_f and n_t typically vary between 0 and 1, with values close to 1 indicating that air and ground surface temperatures are closely related in the cold and warm season, respectively, while low values indicate that they are more disconnected. Note that throughout this study we refer to mean GSTs and

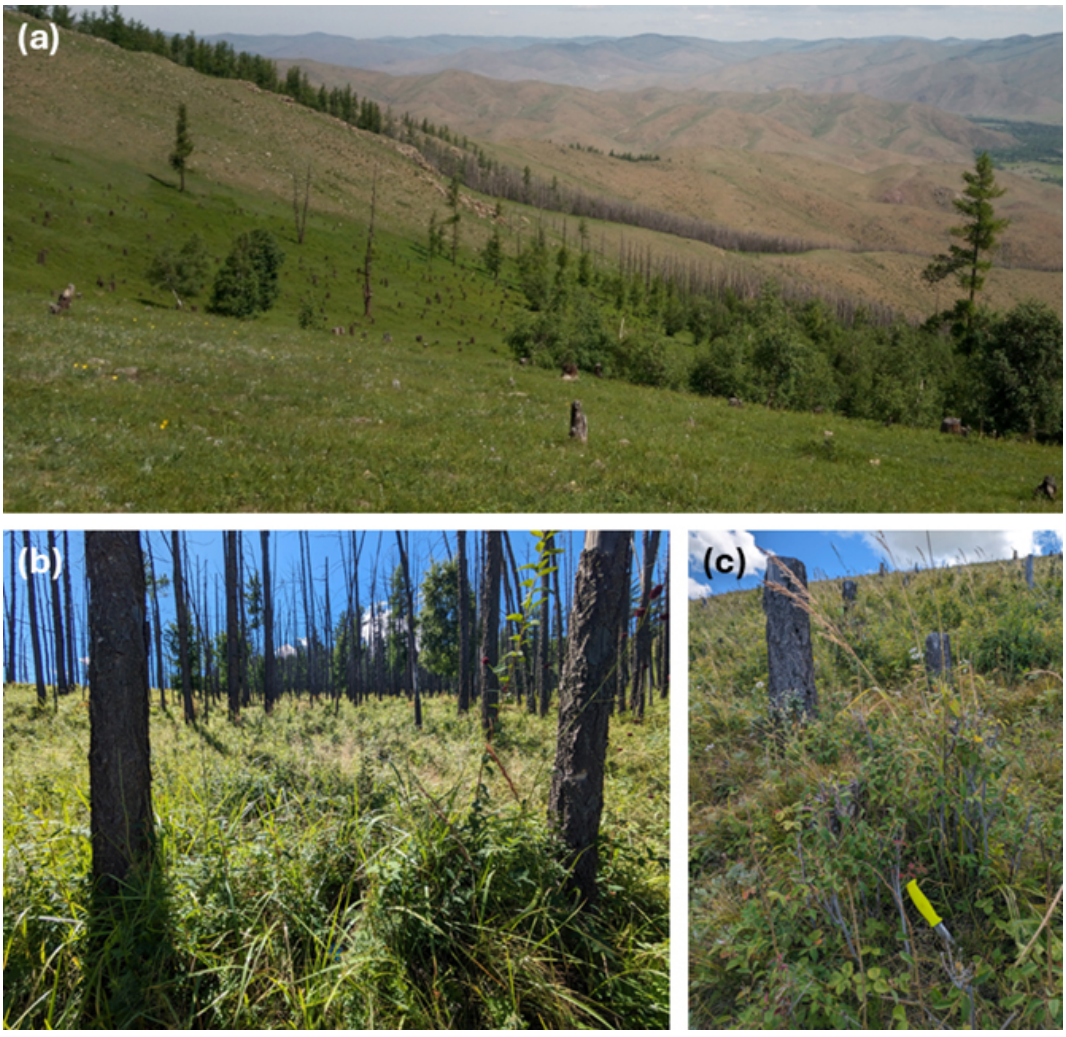

Figure 4. Photographs showing the vegetation cover in the study area. **(a)** 25 June 2022: Looking north from the saddle point close to LOGGED_3, showing the transition from logged and grazed areas in the foreground, to scattered, young regrowth mixed with dead tree trunks in the lower parts of the central valley. The intact and dead forest in the western valley is visible above the ridge in the background. **(b)** 19 August 2023: Dead forest and dense floor vegetation in the vicinity of DEAD_1. **(c)** 19 August 2023: Logged forest at LOGGED_2 with floor vegetation consisting of grasses and shrubs (knife handle 10 cm for scale).

temperature indices by the year in which they end, i.e. SO (2024) in Table 2 is the surface offset over the hydrological year 2024 from September 2023 through August 2024.

2.3 Vegetation density

We quantify vegetation density by estimating the Plant Area Index (PAI) at our field sites from hemispherical images, similar to Zweigel et al. (2024b). The PAI is the total one-sided area of plant material per unit of ground surface and includes both the contribution from live foliage (leaves/needles) and that of woody elements such as stems and branches (Liu et al., 2021). To calculate the PAI from hemispherical images, pixels of vegetation and sky need to be distinguished, and the area of plant material per ground area that would yield such a distribution of vegetation and sky can be calculated. In this study, we use the software Hemisfer (Schleppi et al., 2007) and the methodology by Lang (1987), as well as corrections for slope (Schleppi et al., 2007) and canopy clumping (Chen and Cihlar, 1995), to derive PAI at all sites. While other software/algorithms to derive PAI exist (Liu et al., 2021), and the exact value is influenced by illumination conditions and assumptions regarding vegetation properties (e.g. Thimonier et al., 2010; Zhang et al., 2005), PAIs that are calculated using the same procedures provide a consistent and quantitative measure of vegetation density that can be compared among sites.

At forested sites, the PAI is usually calculated from hemispherical images of the forest canopy only, but in our study area there is also substantial floor vegetation especially at

disturbed sites (Sect. 2.1). We thus calculate the PAI from hemispherical images taken at two levels: (1) 0.5 m above the ground surface and (2) at the ground surface. The former is referred to as "PAI_{canopy}" as it captures the forest canopy only, while the latter includes both the contributions of the forest canopy and floor vegetation and is denoted "PAI_{total}". The hemispheric images from which the PAIs in this study are derived were acquired on 22 December 2022, 6 March 2023 and 19 August 2023.

2.4 Surface cover

We surveyed the surface conditions in the field area in summer and winter. During field visits on 19 August 2023 and 17 September 2024 we measured the height of floor vegetation and the presence of surface organic layers at the ground surface. In winter 2023 we surveyed the snow cover at all sites on 22 December 2022 and 6 March 2023. At the visit in early winter, we took measurements of snow height at each site. In late winter, we observed livestock trampling of the snow cover at the field sites, and we took several measurements of snow height at each site to capture the apparent small-scale variability. We also qualitatively assess the extent of livestock disturbance to the snow cover at the time of visit, which we classify as "scattered" and "extensive" if less than 10 % or more than 50 %, respectively, of the snow surface is visibly disturbed by livestock activity. At the field visit in late winter, we also investigated the presence of litter layers at the base of the snowpack at all sites. Measurements in summer focussed on the immediate vicinity (< 20 cm) of the GST logger location, while observations in winter were generally taken 0.5–2 m away to avoid disturbing the snow cover at the logger location.

2.5 Correlation analysis

We assess the presence of strong relationships between GSTs and various environmental factors through a correlation analysis. This analysis seeks to relate temperature metrics (the target variables) across the 10 field sites to potential explanatory variables. The target variables include annual and seasonal GSTs, the range of seasonal GSTs, and the scale factors for freezing and thawing. As potential explanatory variables we include the measured vegetation densities (including the range of PAI_{canopy}), the thickness of surface organic layers and snow cover, and the various terrain-related metrics presented in Table 1. For the analysis we calculate the Pearson's linear correlation coefficient (abbreviated correlation) without any transformations of the variables, which thus reflects the strength of any linear relationships between the different sets of variables. With a limited sample size of 10, only correlations of above or below 0.7 and -0.7, respectively, are considered strong correlations in the analysis, indicating that the variables share at least half the variance (Janse et al., 2021).

3 Results

3.1 Correlation between GSTs and environmental factors

The correlation analysis (Sect. 2.5) allows for a quantitative assessment of the presence of any strong relationships between GSTs and environmental factors across the disturbance gradient targeted by the field sites. From Table D1 it is evident that the seasonal GST metrics are strongly correlated to vegetation, while there are no strong correlations between MAGST and any of the environmental factors. Specifically, the correlation analysis shows that higher PAI_{canopy} is associated to higher summertime GSTs and lower wintertime GSTs, as well as a smaller seasonal GST range. Interestingly, we do not find any strong correlations between GSTs and the thickness of surface layers of snow or organics. Furthermore, the analysis shows no strong correlations between GSTs and the different terrain metrics, which is expected as the field sites are specifically chosen to have similar terrain characteristics (Sect. 2.1). The lack of strong correlations between terrain metrics and GSTs thus suggests that the remaining terrain variations among the field sites do not substantially influence GSTs. The analysis also shows strong internal correlation within several of the variable types, for example among the different terrain metrics. While that the choice of bounding values of ± 0.7 for correlations to be considered strong (Sect. 2.5) is somewhat arbitrary, we note that the main outcomes of the analysis also hold for more stringent bounding values of for example ± 0.8 (Table D1). Overall, the correlation analysis reveals a strong relationship between seasonal GSTs and vegetation densities among the different forest states at Bayanzurkh.

3.2 Ground surface temperatures

We observe different seasonal evolution of GSTs for the four forest states in the Bayanzurkh mountains. The variability of GSTs with forest state is largest in summer and winter, while GSTs are rather similar among the different forest states in spring and fall (Fig. 5b). During summer, the GSTs in the dead forest and stands of young regrowth are rather similar to those in the intact forest, while the GSTs in the logged forest are circa 1.5 °C higher in both 2023 and 2024. In the cold season the differences in GSTs among the forest states are less systematic, but overall the intact forest and stands of young regrowth feature winter GSTs 2–3 °C higher than the dead and logged forest (Fig. 5b). The largest range in seasonal GSTs is found in the logged forest, spanning from -13.9 to $+13.4$ °C in 2023 (Fig. 5b). In both years the disturbed forest states and the stands of young regrowth feature rather similar MAGSTs, which are 0.5 °C higher than in the intact forest (Fig. 5a). Comparing the two years shows a lower annual GSTs range and higher MAGSTs in 2024 than in 2023 for all forest states, with the latter driven mostly by warmer GSTs

in fall and winter (Fig. 5b). The variability in seasonal GSTs among the 2–3 temperature loggers at each site are generally small (< 1 °C) compared to the GST differences among forest states (Figs. 5b and B2). The largest differences of > 2 °C are observed in summer in the logged forest where we also find the largest spread in PAI_{total} (Sect. 3.3), and in winter and spring where we observe sudden divergences in GSTs at sites subject to livestock trampling (Sect. 3.4, Fig. B1). Similarly, the variability of MAGSTs within each forest states is generally small with the largest values of 1.5–2.2 °C found in the logged forest.

Comparing monthly GSTs from the logged and dead forest to the intact forest sites shows clear seasonal differences (Fig. 6). We find GSTs in the logged and dead forest to be higher than in the intact forest in summer while they are lower in winter. The strongest difference between disturbed sites and intact forest is found in the logged forest, where monthly GSTs are up to -5.1 °C lower and $+3.7$ °C higher than those in the intact forest (Fig. 6). In the dense stands of young regrowth we measure similar or lower GSTs than in the intact forest for most months, except for a short period in early winter in both years (Fig. 6).

In Table 2 we present metrics relating the GST of the different forest states to measured air temperatures. The surface offset (Eq. 1) is close to zero or positive for all forest states in both years, indicating that on annual timescales GSTs are generally higher or equal to air temperatures. Furthermore, the different disturbed forest states have rather similar surface offsets that are circa 0.5 °C lower than for the intact forest in both years. The largest scale factors for both freezing (Eq. 2) and thawing (Eq. 3) are found at the logged forest, which imply that GSTs at these sites more closely follow air temperatures. In both years, the intact forest has the smallest scale factor for freezing while the stands of young regrowth have the smallest scale factors for thawing, indicating that these forest states feature the GSTs that are most disconnected from air temperatures in winter and summer, respectively. Overall, surface offsets are higher and the scale factor for freezing is lower for all forest states in 2024, while the scale factor for thawing is rather similar among the years (Table 2). This indicates that winter rather than summer effects contributed to the higher MAGSTs measured in 2024 (Fig. 5a).

3.3 Vegetation density

The PAI_{canopy} values calculated for the forest states show distinct patterns in vegetation density. Figure 7a shows how the PAI_{canopy} in the intact forest and stands of young regrowth, which both feature live canopies, increases substantially from winter to summer. Particularly, the PAI_{canopy} for the stands of young regrowth increases by 6.3 times from late winter to summer, which is markedly more than the increase in PAI_{canopy} of 4.6 times for the intact forest. We also observe PAI_{canopy} in the intact forest to decrease during winter, which is not observed at any other forest states. This could be linked to gradual shedding of needles, consistent with observation of needles at the snow surface in late winter, or to uncertainties in the PAI calculation under different illumination conditions (see Sect. 4.1). Nevertheless, the difference in wintertime PAI_{canopy} in the intact forest is small (0.5) compared to the PAI increase from early and late winter to summer of 2.2 and 2.7, respectively.

We observe no seasonal evolution in PAI_{canopy} in the dead and logged forest, in line with the absence of live canopies at these sites. In the dead forest we calculate a PAI_{canopy} of 0.4 in winter, which is lower than for intact forest but still a substantial increase compared to the absent canopy of the logged forest (Fig. 7a). In the logged forest the wintertime estimates reveal that the remaining tree stumps do not contribute to PAI_{canopy} (values $\ll 0.1$), and we thus set PAI_{canopy} to 0 also in summer. In the dead forest PAI_{canopy} increases to 0.6 in summer, which is due to scattered regrowth of young trees at the "DEAD_3" site (Sect. 2.1), while the other sites in the dead forest show no increase in PAI_{canopy} in summer (Table C1).

Several of the forest states also feature substantial floor vegetation, which is evident when comparing summertime PAI_{canopy} and PAI_{total} (Fig. 7b). As all forest states feature some floor vegetation, PAI_{total} is greater than PAI_{canopy} at all sites, with an increase in PAI of 1.1 in the intact forest. The smallest increase is found in the stands of young regrowth (0.7), while the largest increase is in the dead forest (3.9). For the logged forest where there is no canopy, we calculate a PAI_{total} of 1.6 which stems entirely from floor vegetation. The variability of PAI_{total} within each forest state is small compared to their absolute value, except for the logged forest where PAI_{total} ranges from 0.9 to 2.5 (Table C1).

Furthermore, we compare vegetation density as quantified by PAI_{canopy} to the scale factors for freezing and thawing (Fig. 8). The scale factors for thawing and freezing are lower for higher summertime and wintertime PAI_{canopy}, respectively, which indicate that GSTs are more disconnected from air temperatures as sites with denser canopies.

3.4 Surface cover

Our observations of surface conditions reveal some general characteristics of the vegetation and snow cover for the different forest states. Snow surveys in December 2022 and March 2023, show mean snow depths of circa 15–20 cm for all forest states at both times, and no systematic differences between the field visits in late December and early March (Fig. C1). The snow cover at all field sites consisted of depth hoar and faceted crystals with no clear horizontal layering. However, we note a substantial increase in livestock disturbance (trampling) to the snow surface from early to late winter (Table 3). While only scattered animal tracks were observed at all sites in December, the snow cover in the dead and logged forest had been substantially altered by animals

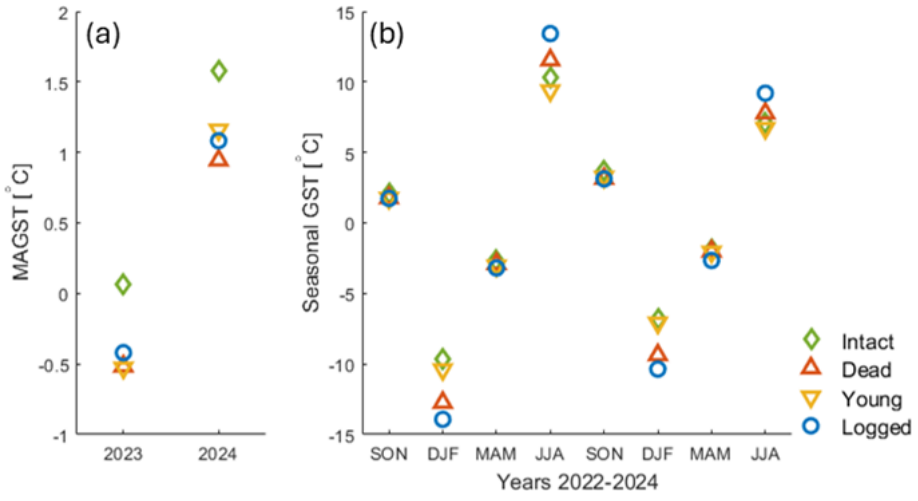

Figure 5. Time series of GSTs for the different forest states in 2023 and 2024. **(a)** depicts mean annual GST while **(b)** shows seasonal GSTs. SON: September, October and November. DJF: December, January and February. MAM: March, April and May. JJA: June, July and August. Note the different scales on the temperature axes of **(a)** and **(b)**. GSTs for the different forest states are presented in Figs. B1 and B2.

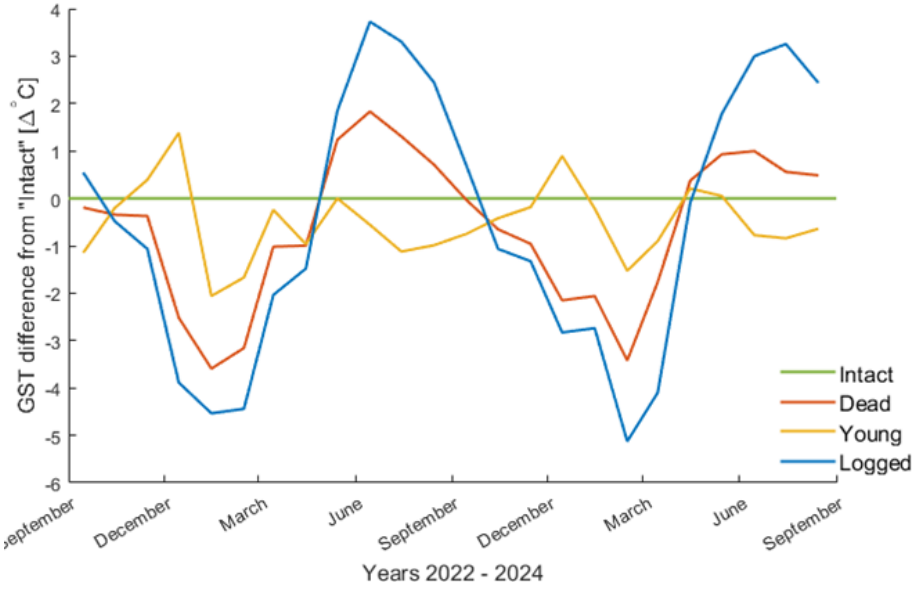

Figure 6. Difference in monthly GST between the disturbed forest states and the intact forest. Positive values indicate that GSTs in the disturbed forest are higher than in the intact forest.

by March, with more than half of the snow surface visually disturbed by animal activity at several field sites. In contrast, we observed only scattered animal tracks in the intact forest throughout winter. In the stands of young regrowth our observations diverge, with extensive trampling observed in the aspen stand (YOUNG_1) in March, while we note only scattered trampling within the larch stand (YOUNG_2). Comparing the average snow depths and the scale factor for freezing for the different forest states reveals no clear relationship (Fig. C2).

Surveys of surface cover show how floor vegetation and surface organic layers vary between the forest states (Table C2). In the intact forest we find floor vegetation of 10–20 cm height underlain by a thin layer of needle litter in both summer and winter. In the stands of young regrowth we observe only sparse floor vegetation and litter layers, while the dead forest features the highest floor vegetation of circa 20–25 cm (Fig. 4b) as well as the thickest litter layers in winter. In the logged forest we find a continuous, 5-15 cm high, grass cover in summer (Fig. 4a), except for at "LOGGED_2" where scattered shrubs yield somewhat higher vegetation

Table 2. Temperature metrics for the different forest states calculated over the hydrological years 2023 and 2024. SO: Surface offset (Eq. 1), n_f: scale factor for freezing (Eq. 2), n_t: scale factor for thawing (Eq. 3).

Forest state	SO (2023)	SO (2024)	n_f (2023)	n_f (2024)	n_t (2023)	n_t (2024)
Intact	0.55	1.05	0.58	0.44	0.64	0.66
Dead	−0.03	0.41	0.74	0.59	0.71	0.69
Young	−0.05	0.63	0.62	0.47	0.58	0.61
Logged	0.06	0.55	0.83	0.68	0.82	0.80

Table 3. Observations of snow cover at the individual field sites. Note that the snow depths on 6 March 2023 are the mean values of several snow measurements. Livestock disturbance is characterized as "scattered" and "extensive" if respectively less than 10 % or more than 50 % of the snow surface are visually disturbed by livestock activity.

Field site	Forest state	22 December 2022		6 March 2023	
		Snow depth	Disturbance	Snow depth	Disturbance
INTACT_1	Intact	21 cm	Scattered	18 cm	Scattered
DEAD_1	Dead	10 cm	Scattered	19 cm	Extensive
DEAD_2	Dead	19 cm	Scattered	16 cm	Extensive
YOUNG_1	Young	21 cm	Scattered	20 cm	Extensive
YOUNG_2	Young	18 cm	Scattered	17 cm	Scattered
DEAD_3	Dead	16.5 cm	Scattered	20 cm	Extensive
LOGGED_1	Logged	20 cm	Scattered	15 cm	Extensive
LOGGED_2	Logged	21.5 cm	Scattered	16 cm	Extensive
LOGGED_3	Logged	17 cm	Scattered	14 cm	Extensive
INTACT_2	Intact	20 cm	Scattered	16 cm	Scattered

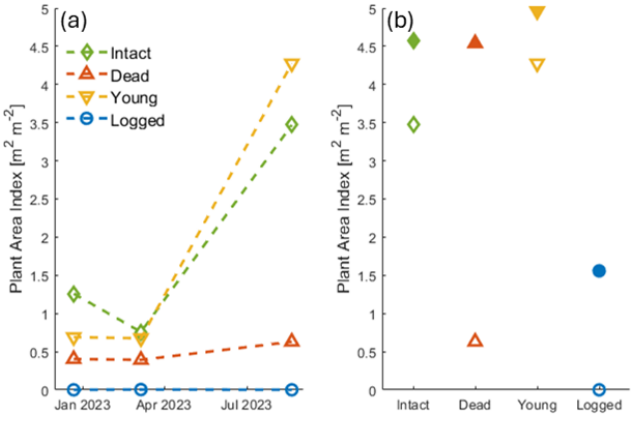

Figure 7. Variations in vegetation densities between the forest states. **(a)** shows the seasonal evolution of PAI_{canopy} in 2023, while **(b)** compares PAI_{canopy} (open markers) and PAI_{total} (filled markers) on the 19 August 2023.

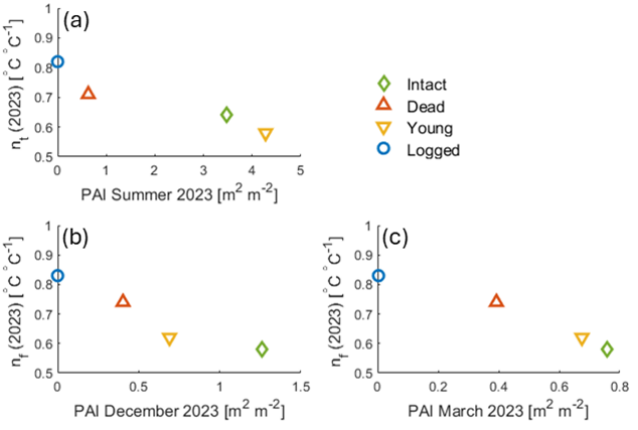

Figure 8. Relationships between vegetation density and the scale factors for freezing and thawing. **(a)** Comparison of summertime PAI_{canopy} (19 August 2023) and the scale factor for thawing (n_t) over the hydrological year 2023. **(b, c)** Comparison of wintertime PAI_{canopy} (21 December 2022 and 6 March 2023, respectively) and the scale factor for freezing (n_f) over the hydrological year 2023.

heights (Fig. 4c). Notably, we find surface organic layers consisting mostly of plant litter at all sites in winter, but at most sites these are thinner or absent in summer (Table C2). Below the layers of surface organics we observe a soil layer containing organics and sand.

4 Discussion

4.1 Novel aspects and limitations

This study presents a novel dataset of GSTs, vegetation density and surface conditions across a forest disturbance gradi-

ent at a site in the forest-steppe ecotone in central Mongolia. Based on these data, we investigate how forest disturbances impact vegetation and surface cover, and the direct and indirect affect that these disturbances have on GST dynamics. Previous studies from the forest-steppe ecotone of central Mongolia have shown a strong dampening of the annual GST cycle and a lowering of MAGSTs associated with forest cover (Dashtseren et al., 2014; Temuujin et al., 2024). However, the ecosystem gradients in these studies occur across substantial differences in topography, and the direct effect of forests on GSTs remains unclear. To untangle the impacts of terrain and ecosystems on ground thermal regime, our study specifically targets differences in forest states across sites with only small differences in topographic characteristics (Table 1). Overall, we find somewhat lower MAGSTs at disturbed sites than in intact forest, while the annual GSTs range is larger at sites where forest disturbances have reduced the canopy cover (Fig. 5).

GSTs in the study area can also be influenced by environmental factors other than forest state, such as differences in topography and floor vegetation. Despite being chosen as to have similar topographic characteristics, there are still variations in terrain among the field sites. For example, the sites of dead forest and stands of young regrowth are located at roughly 50–100 m lower elevation and 2–3° steeper slopes than the intact and logged forest sites (Table 1). Such an elevation difference can entail up to 1 °C higher air temperatures in the lower locations if assuming a dry adiabatic lapse rate (9.8 °C km^{-1}; Hartmann, 2016). The somewhat steeper north-facing slopes in the dead forest and stands of young regrowth can reduce the direct solar radiation at these sites, an effect that is strongest during low solar angles in winter (Table 1). However, we do not observe generally warmer summertime GSTs (nor colder wintertime GSTs) at the dead forest and stands of young regrowth compared to the intact and logged forest (Fig. 5). Moreover, the correlation analysis does not suggest a strong correlation between seasonal GSTs and slope, aspect and elevation, nor available solar radiation (Table D1). Here, we note that while terrain characteristics generally are a main control on GSTs in Mongolian forest-steppe systems (e.g. Temuujin et al., 2024), our study design deliberately uses field sites with similar typographic exposition in order to investigate the impact of forest disturbances specifically (Sect. 2.1). Furthermore, we find variations in floor vegetation within the forest states that potentially affect the measured GSTs. The largest variations in floor vegetation and vegetation density are found in the logged forest, where differences in vegetation height of 25 cm and PAI_{total} of 1.59 are accompanied by a spread in summertime GSTs of 1.8 and 2.5 °C in 2023 and 2024, respectively. However, we find that despite the variations within the logged forest, LOGGED_1, LOGGED_2 and LOGGED_3 still have the lowest PAI_{total} and highest summertime GSTs of all field sites. This indicates that the impact of variations in topography among the forest states, and vegetation cover within the forest states, is small compared to the control of forest states on GSTs.

In this study we describe the vegetation density using the plant area index (PAI), which despite its broad use has inherent limitations. The PAI was chosen as it gives a single, quantitative vegetation metric per site/field visit, and easily can be estimated using non-destructive optical methods and off-the-shelf software that accounts for relevant effects such as local slope and canopy clumping (Sect. 2.3). As the PAI includes all plant material, it is a useful measure of the canopy-atmosphere interface and a suitable metric for e.g. overall light transmission in forests. However, factors such as exposure and sky conditions influence the estimation of PAI (Chen et al., 1991), which can have contributed to the drop of 0.5 in PAI_{canopy} in the intact forest in winter (Fig. 7). Furthermore, the PAI has limited application in fields such as hydrology and ecology, as processes such as transpiration and photosynthesis occur only through the leaf-/needle-area (Bréda, 2003), while accurate modelling of sub-canopy radiation relates more to the sky-view fraction and the transmissivity of direct solar radiation (Jonas et al., 2020). In principle, these vegetation metrics can be derived from the hemispherical images using established methodologies, e.g. the leaf area index (LAI) of the canopy can be found as the difference in PAI_{canopy} between summer and winter.

GSTs are also influenced by atmospheric factors such as air temperature and precipitation, which can vary from year to year. Meteorological data from the nearby Nalaikh station shows MAAT between −3.4 and −2.3 °C during the study period, which is near or above the 2000–2024 average (Sect. 2.1). Annual precipitation was above average during the study period, with the calendar year 2024 being the wettest year in the 25-year record (Fig. 2). However, both MAAT and precipitation show an increasing trend over the 2000–2024 period (Fig. 2), which is expected to continue over the next decades (Zamba, 2018). It is thus likely that the relationships between vegetation cover and GSTs established in this study period also are relevant for climatic conditions in the near future. Furthermore, we measure a MAAT of −0.2 °C at the ridge above the study area in 2023 (Sect. 2.1, Fig. 1a), which is 2.9 °C higher than the corresponding MAAT recorded in Nalaikh (Fig. 2). This difference is linked to the strong temperature inversions that are frequent during winter in this region (Gerelchuluun and Ahn, 2014). Radiosonde data have shown that temperature inversion around Ulaanbaatar are common from October through March with strengths up to 6.9 °C (Ganbat and Baik, 2016; Sumiya et al., 2023). The persistence of such inversions throughout the cold season can produce systematically lower wintertime air temperatures in valleys and topographic depressions, i.e. where Nalaikh is situated, compared to our study area which is located at higher altitude close to the mountain ridge (Fig. 1a). This suggests that relative position within the larger scale terrain needs to be considered when comparing temperature data in this region.

More systematic surveys of snow cover are required for quantifying its impact on GST dynamics. The survey in late winter reveals a snow cover that is substantially disturbed by livestock at several of the field sites, especially in the dead and logged forest (Table 3). We classify this disturbance as "scattered" and "extensive" based on the percentage of snow surface that is visually disturbed by livestock activity (Sect. 2.4). Such a classification is however not suitable for the correlation analysis (Sect. 3.4), and our further discussion of the role of livestock disturbances in shaping wintertime GSTs remains qualitative. Furthermore, our snow sampling does not capture events where previously disturbed areas are infilled by subsequent snowfalls. However, a more comprehensive and quantitative assessment of livestock disturbance was not possible within the scope of this study. Future research efforts could for example use repeated airborne LiDAR surveys in winter for detailed snow depth mapping (Koutantou et al., 2022), which could provide information on the snow depth evolution at the location of the GST measurements, and be used to analyse the extensiveness of snow trampling within each forest state.

4.2 Factors impacting ground surface temperature dynamics in disturbed forests

A key effect of forest canopies is the attenuation of solar radiation, which reduces the available energy at the ground surface (e.g. Mahat and Tarboton, 2012; Stuenzi et al., 2021a). The shading effect scales with canopy density, for example, Dashtseren et al. (2014) found that for a site near our study area only 14 %–22 % of the incoming solar radiation penetrated the forest canopy in summer, while corresponding values for the leaf-less season where 63 %–67 %. Overall, disturbances that remove or reduce the canopy density will increase the solar radiation available at the ground surface which can give higher GSTs, an effect which is strongest during high insolation in summer. This is in line with the correlation analysis, which shows a strong relationship between vegetation density and summertime GSTs and the scale factor for thawing (Eq. 3, Table D1), with the lowest summertime GSTs and n_t values found at sites with higher summertime PAI_{canopy} (Figs. 5 and 7a).

Forest canopies can also intercept substantial amounts of solar radiation in winter, which affects the surface energy balance at forested sites. In the forest-steppe ecotone, forests consist mainly of deciduous needle-leaves and are located on north-facing slopes (Schlütz et al., 2008; Tsogtbaatar, 2004). During winter, when sun angles are lower and forest canopies have shed their needles, incoming solar radiation has both a longer travel distance through the canopy while also being able to penetrate deeper into the canopy. For similar latitudes as our sites, Webster et al. (2015) showed that larch tree trunks in winter are warmer than the surrounding air, emitting substantial amounts of longwave radiation to the snow surface. At times when absorption of solar radiation is limited by highly reflective snow cover, sites with dark tree trunks can thus experience increased energy input to the local surface. This tendency of more available energy at forested sites in winter agrees well with our findings of higher wintertime GST and lower scale factor for freezing (Eq. 2) at sites with denser canopies (Fig. 8b, c) and the strong positive correlations between PAI_{canopy} and wintertime GSTs (Table D1).

The exchange of energy between the atmosphere and ground at forested sites can also be modified by the presence of surface organic layers, which in our study area consist mostly of needle- and grass litter (Table C2). The low thermal conductivity of such layers efficiently insulates the soil below, which affects the ground thermal regime through dampening of the annual ground temperature range and maintaining shallow active layer thickness' (Beringer et al., 2001; Bonan and Shugart, 1989; Chang et al., 2015; Kasischke and Johnstone, 2005). For the forest-steppe ecotone, thick surface organic layers are observed in intact forests and at grassland sites where grazing is limited (Dashtseren et al., 2014; Ishikawa et al., 2005; Zweigel et al., 2024b) while they are shallow at sites with degraded forest or young regrowth (Klinge et al., 2021). In this study we measure GSTs below the surface organic layer (Sect. 2.2), and any effects of such layers are contained in the GST records. Overall, we observer rather thin (0–5 cm) surface organic layers in our study area, where needle litter are found year-round in the intact forest, while grass- and leaf litter layers are found in winter only at the disturbed forest sites (Table C2). This diminishing of surface organic layers throughout the year could be due to animal foraging of plan litter (see below), gradual settling, or decomposition which can be substantial already within the first year (Zhao et al., 2022). However, the correlation analysis does not indicate any strong relationships between the surface organic layer thickness and seasonal GSTs nor the scale factors for freezing and thawing. This suggests that variations in surface organic layer thickness among the forest states are not the dominant factor influencing GST dynamics in our study area.

An interesting finding is that dead forest has similar PAI_{total} as the intact larch forest (Fig. 7b) but features higher summertime GSTs (Fig. 5). This GST difference is observed despite grassland vegetation (which dominate the dead forest) having generally higher summer albedo than coniferous forest (to which larches belong) (Bonan, 2016), indicating lower absorption of solar radiation in the dead forest. While the exact reasons for these differences are unclear, there are notable difference in vegetation structure between these sites which can have implications for the processes by which energy is transfers from the vegetation to its surroundings. In the intact forest the largest part of the vegetation density is in the tall tree canopy, while it is in the floor vegetation in the dead forest (Fig. 7b). This implies that the absorption of solar radiation (and consequent heating of the vegetation) occurs much closer to the ground surface in the dead forest than in the intact forest, resulting in a larger temperature gradient

between the vegetation and ground surface and subsequently more efficient energy transfer at this site. Furthermore, the relatively open canopy air space in the intact forest, and the exposure to greater wind speed higher up, can allow the intact forest canopy to more efficiently shed heat to the atmosphere.

Our results contrast some of the previous research on the impact of forest disturbances on the ground thermal regime. Generally, forest disturbances have been shown to increase ground temperatures, potentially leading to permafrost degradation (e.g. Fedorov et al., 2017; Iwahana et al., 2005; Li et al., 2021; Yoshikawa et al., 2002). For the forest-steppe ecotone of central Mongolia, Klinge et al. (2021) and Kopp et al. (2014) found summertime GSTs at sites affected by wildfire that were 3.1 to 3.9 °C warmer compared to nearby intact forest. Year-round studies of wildfires and clear-cuttings found that reduced evapotranspiration following disturbances strongly increased soil moisture levels, which delayed freezing and deepened the active layer (Fedorov et al., 2017; Iwahana et al., 2005; Yoshikawa et al., 2002). In our study area, we observe a similar increase in summertime GST at disturbed sites as Klinge et al. (2021) and Kopp et al. (2014), but this warming is offset by overall lower GSTs in winter, and we do not observe slower freezing at disturbed sites (Figs. 5b and B2). The correlation analysis also does not show any strong correlations between MAGST and the variations in surface and vegetation cover across the different forest states (Table D1). Overall, our two years of measurements show an increased annual GST cycle and MAGSTs consistently 0.5 °C lower at disturbed sites compared to intact forest (Fig. 5). Unlike the study sites of Yoshikawa et al. (2002), Iwahana et al. (2005) and Fedorov et al. (2017), our study area is located on discontinuous permafrost in sloping terrain, which could give a more efficient drainage of soil water and thus inhibit the buildup of soil moisture following disturbances. While we do not have observations at deeper ground layers, this demonstrates that forest disturbances do not necessary lead to warming of ground temperatures, and that their impact on ground thermal regime is influenced by the local hydrological regime.

Furthermore, differences in grassland vegetation impact GST dynamics, which can explain the differences observed in the dead and logged forest. These sites feature similar topographic characteristics (Table 1), but we observe lower PAI_{total} and only negligible layers of surface organics in the logged forest (Fig. 7, Table C2). Such a sparser surface cover intensifies the exchange of energy between the atmosphere and ground surface (Zweigel et al., 2024b), which is in line with the higher summertime GSTs and larger scale factor for thawing observed in the logged forest (Figs. 4 and 8b). It is likely that these differences in summertime surface cover are due to livestock grazing, as we observe several active herder camps on south-facing slopes in the immediate surroundings of our study area (< 2 km) and the logged forest is easily accessible from the south (Fig. 1a).

During winter the presence and depth of the snow cover can substantially limit the exchange of energy between the atmosphere and ground surface, exerting significant control on the overall ground thermal regime (Zhang, 2005). Previous works have shown that snow cover can vary substantially between sites with different vegetation cover, which can be due to (a) snow capture, where interactions between wind and vegetation cover create areas of preferential snow accumulation at sites with higher and denser vegetation (Hiemstra et al., 2002; Sturm et al., 2001), and (b) interception loss, where denser canopies intercept more snow (Fisher et al., 2016; Lundberg and Koivusalo, 2003; Yi et al., 2007). Due to these effects on snow accumulation, variations in vegetation densities due to forest disturbances can lead to substantial differences in wintertime ground temperatures, an effect that is strongest at sites with overall thin snow cover (Li et al., 2021; Zhang, 2005). Interestingly, we observe rather similar snow depths for the different forest states in Bayanzurkh (Fig. C1) and find no clear relationship between observed snow depth and n_f (Fig. C2) nor a strong correlation between snow depths and wintertime GSTs (Table D1). This lack of systematic differences in snow cover between the forest states could be linked to limited wind redistribution of snow due to the overall sheltered location of the field sites (Sect. 2.1) and the generally low wintertime windspeeds in central Mongolia (Hong et al., 2023), and the deciduous nature of the forest in our field area, which limits snow interception. Notably, the main difference in snow cover between the forest states is the degree of livestock trampling, which is characterized as scattered in the intact forest and extensive in the dead and logged forest (Table 3). If trampling leads to compaction of the entire snowpack, this can substantially reduce the thermal insulation of snow and give lower wintertime GSTs (e.g. Zweigel et al., 2024b). For both the dead and logged forest, the temperature records show sudden divergences in GST for single loggers in winter (Fig. B1). A similar divergence in GSTs is also evident for the stand of young aspen, where we also note extensive disturbance by livestock (Table 3). While we do not have direct observations linking these GST signals to trampling, the extent of trampling observed at the sites in the dead and logged forest suggest that livestock disturbances to the snow cover can contribute to the overall colder winter GSTs at these sites.

Overall, livestock activity influences surface conditions in our study area, and these must be considered when studying the differences in GST dynamics between the forest states. While the exact patterns of livestock activity are unclear, we note some general tendencies; in summer, the sparser vegetation cover in the logged forest suggests that these sites are preferentially grazed (Fig. 7b), while the more abundant trampling at the dead and logged forest and the stand of young aspen indicates larger livestock activity at these sites in winter (Table 3). The latter is likely linked to the abundance of edible grass and leaf litter at these sites contrary to the needle litter that dominates both young and in-

tact larch forests (Table C2). For a north-facing grassland site in central Mongolia, Zweigel et al. (2024b) found grazing and trampling by livestock to give 1.4 °C warmer and 2.5 °C colder GSTs in summer and winter, respectively, and an overall cooling of MAGST of 0.4 °C. It is thus likely that livestock activity contributes to the larger annual GST cycle and lower MAGSTs in the logged and dead forest sites compared to the intact forest (Fig. 5). As these impacts are superimposed on the forest disturbances in our study area, quantification of their contribution to the observed GST dynamics is not possible. However, livestock activity likely also affects surface conditions throughout the forest-steppe ecotone, as 70 %–80 % of the Mongolian land area is used as rangeland (Angerer et al., 2008; Fernández-Giménez et al., 2018) and forests constitute important feeding grounds that are used especially in winter (Lkhagvadorj et al., 2013b, a).

4.3 Implications and future work

In the forest-steppe ecotone both permafrost and forest are close to their climatic limits and their existence is intimately linked (e.g. Dashtseren et al., 2014; Klinge et al., 2018). In its intact state, forest ecosystems provide shade and insulation which limit ground thawing in summer, while the presence of shallow permafrost elevates the water table and increases local soil moisture levels. The potential for these systems to reestablish themselves after disturbances has received little attention, except for the work by Klinge et al. (2021). For burnt and exploited forests in central Mongolia, they found an overall drying of the soil and deepening of the active layer. Modelling efforts have since underpinned the impact removal of forest canopy and associated surface organic layers have on soil moisture and seasonal thaw depth (Zweigel et al., 2024a). Such ground conditions are unfavourable for tree saplings, and initial succession is limited to topographic formations promoting water availability (Klinge et al., 2021). We also observe this effect in our study area, where sparse regrowth is found across the parts facing directly north, whereas stands of dense young regrowth (e.g. YOUNG_1 and YOUNG_2) are limited to topographic concavities (Fig. 1). However, these stands of young regrowth feature the coldest summertime GSTs and the lowest scale factor for thawing (Fig. 5b, Table 2), indicating a limited active layer thickness and locally stable permafrost at these sites. Such stands of young regrowth might be essential for the gradual regeneration of forest on disturbed slopes, as they provide necessary soil moisture and seed reservoir (Klinge et al., 2021). Fully understanding and quantifying the role of permafrost-ecosystem interactions for regenerating/degenerating forests is however beyond the scope of our study at this time and should be a topic for future research.

The observed variation in GST dynamics between the different forest states can impact the local ground thermal regime. Overall, we find about 0.5 °C lower surface offset (Eq. 1) in the dead and logged forest and stands of young regrowth compared to the intact forest (Table 2), indicating a general cooling of the ground surface following forest disturbance. However, the dead and logged forest also have a larger annual GST amplitude (Fig. 5b), which in turn can increase the thermal offset and give higher ground temperatures at depth (Smith and Riseborough, 1996). Due to the potentially opposing effects of surface- and thermal offset, the impact of dead or logged forest on deeper ground temperatures remains unclear.

The abundant growth of floor vegetation at disturbed forest sites might limit remote sensing efforts in assessing the spatial scale of forest disturbance. Most remotely sensed vegetation indexes (i.e. NDVI) are based on the ratio between different spectral bands and thus do not distinguish between vegetation in the canopy and at the forest floor (Glenn et al., 2008). At our sites, we observe abundant grass vegetation in disturbed sites, yielding rather similar PAI_{total} for intact and disturbed forest (Fig. 7b). Also previous works have found common vegetation indexes to be insensitive to disturbances in larch forest, as loss of canopy cover is compensated for by increased vitality of floor vegetation (Bendavid et al., 2023; Loranty et al., 2018). This suggests that vegetation indices derived from spectral remote sensing products might be inadequate for detecting or mapping the spatial extent of such forest disturbances and for assessing their impact on GSTs.

This observed relationship between vegetation density and GSTs suggests that canopy effects need to be considered when simulating permafrost in forest ecosystems. In recent years, single- or multi-layer vegetation schemes that directly account for canopy effects have been integrated in existing permafrost models and applied at the point scale (e.g. Stuenzi et al., 2021a, b; Zweigel et al., 2024a). However, the faster and simpler models used to simulate regional and global permafrost extent often lump the effects of vegetation, snow cover and surface organics into scale factors linking air and ground surface temperatures (e.g. Jafarov et al., 2012; Obu et al., 2019; Westermann et al., 2015). In the frequently used permafrost map by Obu et al. (2019), direct canopy effects are not considered in the parameterization of the scale factors for freezing and thawing, and this is pointed out as a main source of uncertainty in the representation of permafrost extent in forested regions. However, the clear relationship between canopy density and the scale factors for thawing and freezing found in this study (Fig. 8) shows that canopies have a strong control on GSTs throughout the year. At our study sites, the impact of canopies on freezing and thawing largely cancel each other out, and surface offsets vary only by 0.5 °C with forest state (Table 2). However, the strength of canopy effects such as shading, interception and snow capture vary with geographic location, climate and forest type, and should be considered in future permafrost mapping efforts.

The observed GST dynamics in the logged and dead forest are likely to affect the soil moisture regime, with important implications for ecosystem function. Specifically, higher summertime GSTs and larger annual GST range are typi-

cally associated with a deepening of the active layer (Smith and Riseborough, 1996; Zhang et al., 1997), and greater active layer thicknesses have been observed at disturbed forest sites in central Mongolia (Klinge et al., 2021). As permafrost is largely impermeable (Walvoord and Kurylyk, 2016), a deeper active layer permits water infiltration to greater depths while higher summertime GSTs at the same time increase surface evaporation. Consequentially, near-surface moisture levels are reduced which limits water available for plant uptake. Moreover, meltwater from ground ice near the top of the permafrost can be crucial in sustaining boreal forests during dry years (Sugimoto et al., 2002). If forest disturbances lead to deepening of the active layer and a melt out of these ground ice layers, this important water reservoir is lost and any post-disturbance ecosystems will be more susceptible to droughts. Overall, forest disturbances can negatively affect both short- and long-term water availability, which has implications for ecosystem function and succession. Although investigating water availability is beyond the scope of this study, the similar terrain configurations among sites in the Bayanzurkh mountains suggest that it could be a well-suited location for future research on the impact of forest disturbances on soil moisture dynamics.

5 Conclusion

In this study we explore the relationship between ground surface temperatures (GST), vegetation density and surface cover at intact and disturbed forest sites in the discontinuous permafrost in central Mongolia. We present two years of daily GST measurements from sites with intact, dead, and logged forest, as well as from dense stands of young regrowth. The GST measurements are complemented by daily air temperature measurements, calculations of canopy and floor vegetation density and surveys of surface cover in summer and winter.

We find forest disturbances to strongly affect vegetation structure, with the dead and logged forest featuring lower canopy density, denser floor vegetation and lower accumulation of surface organic layers. Stands of young regrowth have the highest summertime canopy density and the sparsest floor vegetation, and feature only a negligible surface organic layer. The forest disturbance also induces differences in local livestock activity especially in winter when grass- and leaf litter available at disturbed sites is an important source of feed. Overall, there is a clear relationship between canopy density and winter and summer GSTs, where the annual GST amplitude increases at sites with sparser canopies. Compared to intact forest, monthly GSTs in the dead and logged forest are up to $+1.8$ and $+3.7$ °C higher in summer and up to -3.6 and -5.1 °C lower in winter, respectively. In stands of young regrowth, GSTs are generally lower and more dampened than in intact forest. We find summer and winter effects to largely offset each other, and that mean annual GSTs in the dead, logged and stands of young regrowth are 0.5 °C lower than in the intact forest.

Our findings suggest that while forest disturbances strongly influence the GST dynamics, they do not lead to widespread warming of the ground surface or permafrost degradation. Forest disturbances lead to a shift in vegetation density from the canopy to the forest floor, which can impede remote sensing of forest disturbances using well-established vegetation indices and induce patterns in livestock activity.

Appendix A: Location of the field sites

Table A1. Coordinates of the field sites used in this study.

Logger	Latitude [°]	Longitude [°]
INTACT_1	47.8334	107.2137
DEAD_1	47.8348	107.2165
DEAD_2	47.8336	107.2175
YOUNG_1	47.8333	107.2179
YOUNG_2	47.8326	107.2190
DEAD_3	47.8326	107.2193
LOGGED_1	47.8295	107.2202
LOGGED_2	47.8294	107.2206
LOGGED_3	47.8303	107.2174
INTACT_2	47.8324	107.2129

Appendix B: Time series of GST evolution

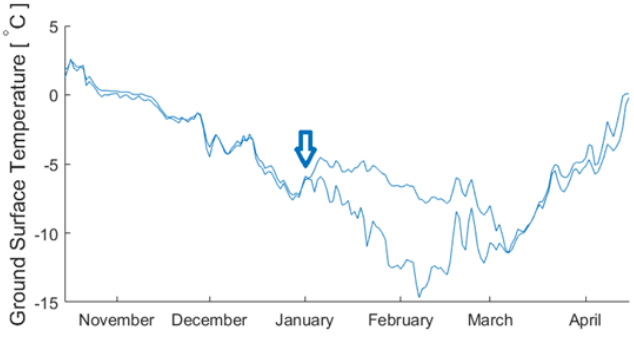

Figure B1. Evolution of daily GSTs for the individual loggers in the young forest stands winter 2024. The arrow indicates a time in late December from which the two loggers swich from having highly similar GSTs to having strongly diverging GSTs until late winter, possibly in response to livestock trampling at the young aspen site (YOUNG_1).

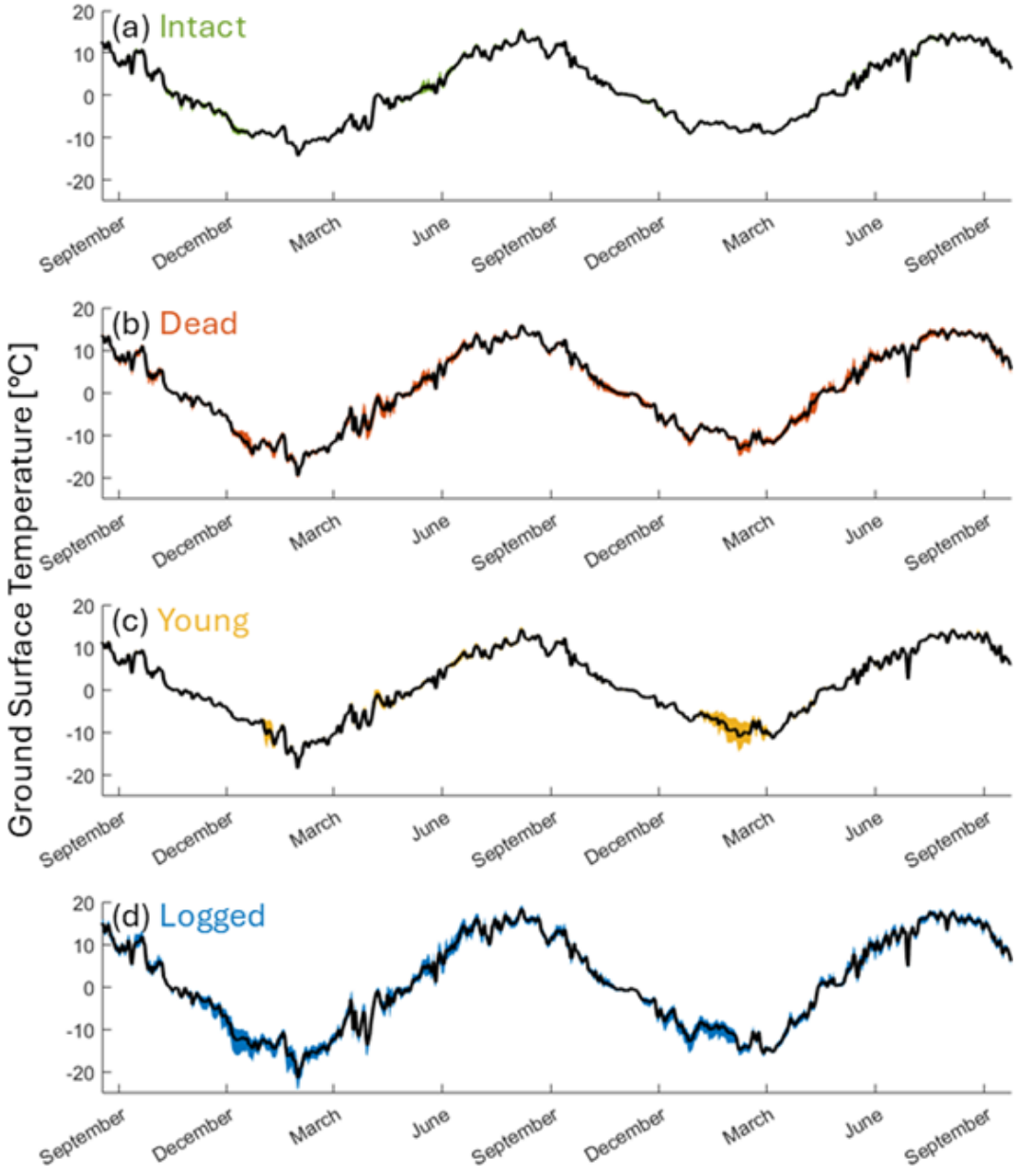

Figure B2. Daily mean GST (black line) and GST range (coloured shading) for the 2–3 temperature measurements within the different forest states (Sect. 2.2). Note the abrupt increases in GST range in winter for some forest states, which is due to sudden divergence in GST for single loggers.

Appendix C: Detailed vegetation and snow observations

Table C1. Calculated PAI for the different field sites.

Logger	Forest state	PAI_{canopy}			PAI_{total}
		22 Dec 2022	6 Mar 2023	19 Aug 2023	19 Aug 2023
INTACT_1	Intact	1.15	0.77	3.60	4.20
DEAD_1	Dead	0.30	0.32	0.34	4.94
DEAD_2	Dead	0.40	0.41	0.40	4.51
YOUNG_1	Young	0.58	0.63	4.14	5.39
YOUNG_2	Young	0.80	0.73	4.41	4.53
DEAD_3	Dead	0.51	0.45	1.15	4.17
LOGGED_1	Logged	0.00	0.00	0.00*	2.45
LOGGED_2	Logged	0.00	0.01	0.00*	1.38
LOGGED_3	Logged	0.00	0.00	0.00*	0.86
INTACT_2	Intact	1.37	0.75	3.35	4.94

* PAI_{canopy} values for logged sites in summer are not calculated directly but are assumed to be equal to those calculated for winter (see Sect. 3.2).

Table C2. Observed surface cover from the visits in 6 March 2023, 19 August 2023 and 17 September 2024. Note that the surface organic layer was only qualitatively assessed in summer 2024.

Field site	Floor vegetation		Surface organic layers		
	2023 summer	2024 summer	2023 winter	2023 summer	2024 summer
INTACT_1	n.m.	n.m.	1 cm, litter	4 cm, litter	Needle litter
INTACT_2	10–20 cm, grass	n.m.	1–2 cm, litter	1 cm, litter	Needle litter
DEAD_1	25 cm, grass	20 cm, grass	5 cm, grass litter	0 cm	Grass litter
DEAD_2	25–50 cm, grass	20 cm, grass	5 cm, grass litter	0 cm	Grass litter
DEAD_3	25 cm, grass	15 cm, grass	2 cm, litter/moss	1 cm, moss	Litter and moss
YOUNG_1	3–4 m, Aspen saplings	0 cm, grass	2 cm, litter	0 cm	Leaf litter
YOUNG_2	2–4 m, Larch saplings	n.m.	2 cm, litter	0 cm	Needle litter
LOGGED_1	15 cm, grass	15 cm, grass	5 cm, litter/moss	0 cm, 10 %–20 % bare soil	Negligible
LOGGED_2	20–30 cm, grass/shrubs	40 cm, grass/shrubs	2 cm, grass litter	0 cm, 10 %–20 % bare soil	Negligible
LOGGED_3	5–15 cm, grass	15 cm, grass	1 cm, grass litter	0 cm	Negligible

n.m.: not measured.

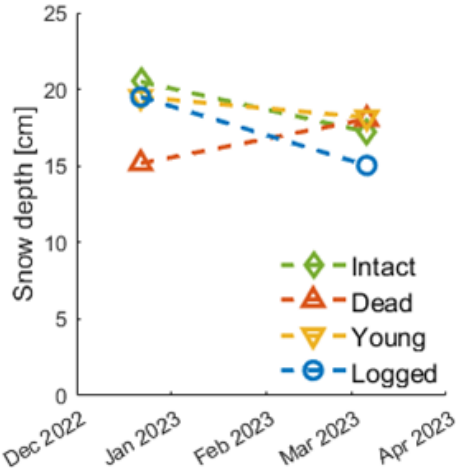

Figure C1. Average snow depths measured in the immediate vicinity of the logger locations in winter 2023. Note that the data from 6 March 2023 is the mean of measurements at both visually undisturbed and disturbed locations.

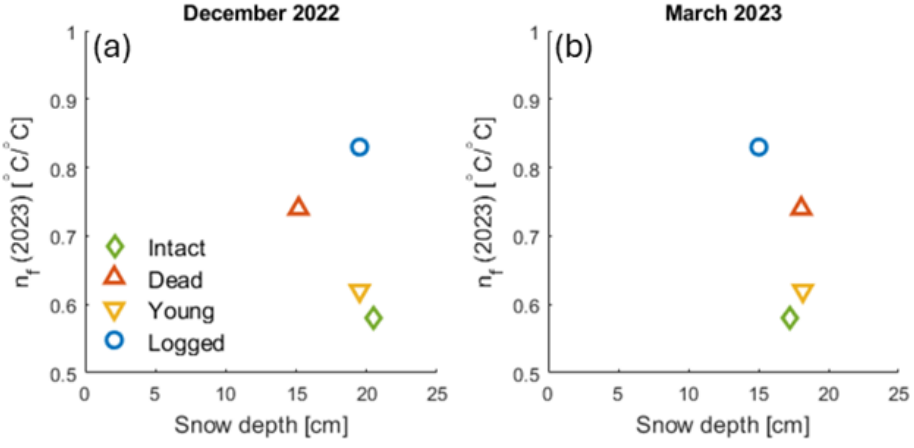

Figure C2. Comparison of average snow depth and the scale factor for freezing (n_f) over the hydrological year 2023.

Table D1. Correlation between temperature indices and various metrics related to vegetation and surface cover, and terrain for the hydrological year 2023. Here, the temperature indices are considered target variables (italic font), while the different vegetation, surface and terrain metrics (normal font) are considered possible explanatory variables. Correlations above or below 0.7 and −0.7, respectively, are considered strong correlations, and these are indicated by bold font. GST_{range} refers to the difference between summer and wintertime GSTs, while d_{SOL} and d_{snow} are the depth of the surface organic layer and snow cover, respectively. For variables that relate to a specific time or period, this is indicated in brackets. S_{in} is considered a terrain metric as the field sites are situated in close spatial proximity, so that differences in available solar radiation are induced by terrain variations between the sites.

		Temperature indices						Vegetation density					Surface cover				Terrain metrics						
		MAGST	$GST^{(Winter)}$	$GST^{(Summer)}$	GST_{range}	n_f	n_t	$PAI_{canopy}^{(Dec)}$	$PAI_{canopy}^{(Mar)}$	$PAI_{canopy}^{(Aug)}$	$PAI_{canopy}^{(Aug-Mar)}$	$PAI_{total}^{(Aug)}$	$d_{SOL}^{(Mar)}$	$d_{SOL}^{(Aug)}$	$d_{snow}^{(Dec)}$	$d_{snow}^{(Mar)}$	Elevation	Slope	Aspect	SVF	S_{in}	$S_{in}^{(Winter)}$	$S_{in}^{(Summer)}$
Target variables	*MAGST*	**1.00**	0.50	0.17	−0.21	−0.63	0.30	0.23	0.14	0.09	0.08	0.25	0.51	0.22	0.38	−0.16	0.20	0.16	−0.61	−0.06	0.06	0.08	0.07
	$GST^{(Winter)}$	0.50	**1.00**	**−0.74**	**−0.94**	**−0.97**	−0.66	**0.84**	**0.85**	**0.83**	**0.80**	**0.70**	−0.14	0.46	0.43	0.41	0.05	0.61	−0.32	−0.41	−0.60	−0.57	−0.59
	$GST^{(Summer)}$	0.17	**−0.74**	**1.00**	**0.92**	0.65	**0.99**	**−0.77**	**−0.89**	**−0.86**	**−0.83**	**−0.74**	0.39	−0.24	−0.05	−0.60	0.21	−0.64	0.02	0.54	0.69	0.65	0.69
	GST_{range}	−0.21	**−0.94**	**0.92**	**1.00**	**0.88**	**0.87**	**−0.86**	**−0.93**	**−0.90**	**−0.87**	**−0.77**	0.27	−0.39	−0.27	−0.53	0.07	−0.67	0.19	0.50	0.68	0.65	0.68
	n_f	−0.63	**−0.97**	0.65	**0.88**	**1.00**	0.55	**−0.77**	**−0.79**	**−0.74**	**−0.72**	**−0.75**	−0.06	−0.37	−0.38	−0.37	0.00	−0.63	0.49	0.46	0.50	0.46	0.49
	n_t	0.30	−0.66	**0.99**	**0.87**	0.55	**1.00**	**−0.71**	**−0.83**	**−0.82**	**−0.79**	−0.65	0.48	−0.22	−0.06	−0.63	0.21	−0.60	−0.06	0.50	0.68	0.65	0.68
Explanatory variables	$PAI_{canopy}^{(Dec)}$	0.23	**0.84**	**−0.77**	**−0.86**	**−0.77**	**−0.71**	**1.00**	**0.93**	**0.81**	**0.77**	0.68	−0.37	0.62	0.21	0.34	0.29	0.36	−0.03	−0.18	−0.47	−0.46	−0.45
	$PAI_{canopy}^{(Mar)}$	0.14	**0.85**	**−0.89**	**−0.93**	**−0.79**	**−0.83**	**0.93**	**1.00**	**0.89**	**0.85**	**0.83**	−0.31	0.51	0.13	0.55	−0.05	0.54	−0.04	−0.46	−0.61	−0.58	−0.60
	$PAI_{canopy}^{(Aug)}$	0.09	**0.83**	**−0.86**	**−0.90**	**−0.74**	**−0.82**	**0.81**	**0.89**	**1.00**	**1.00**	0.64	−0.49	0.39	0.33	0.47	0.02	0.39	0.05	−0.29	−0.51	−0.51	−0.52
	$PAI_{canopy}^{(Aug-Mar)}$	0.08	**0.80**	**−0.83**	**−0.87**	**−0.72**	**−0.79**	**0.77**	**0.85**	**1.00**	**1.00**	0.59	−0.51	0.36	0.36	0.45	0.03	0.35	0.07	−0.25	−0.48	−0.48	−0.49
	$PAI_{total}^{(Aug)}$	0.25	**0.70**	**−0.74**	**−0.77**	**−0.75**	−0.65	0.68	**0.83**	0.64	0.59	**1.00**	0.19	0.19	−0.18	0.68	−0.40	**0.77**	−0.38	**−0.77**	−0.58	−0.50	−0.58
	$d_{SOL}^{(Mar)}$	0.51	−0.14	0.39	0.27	−0.06	0.48	−0.37	−0.31	−0.49	−0.51	0.19	**1.00**	−0.44	−0.39	−0.14	−0.42	0.32	−0.61	−0.41	0.08	0.16	0.08
	$d_{SOL}^{(Aug)}$	0.22	0.46	−0.24	−0.39	−0.37	−0.22	0.62	0.51	0.39	0.36	0.19	−0.44	**1.00**	0.26	0.26	0.44	−0.07	0.04	0.18	−0.07	−0.12	−0.07
	$d_{snow}^{(Dec)}$	0.38	0.43	−0.05	−0.27	−0.38	−0.06	0.21	0.13	0.33	0.36	−0.18	−0.39	0.26	**1.00**	−0.13	0.38	−0.17	−0.04	0.28	0.02	−0.05	0.02
	$d_{snow}^{(Mar)}$	−0.16	0.41	−0.60	−0.53	−0.37	−0.63	0.34	0.55	0.47	0.45	0.68	−0.14	0.26	−0.13	**1.00**	−0.55	0.68	−0.15	**−0.72**	−0.58	−0.54	−0.61
	Elevation	0.20	0.05	0.21	0.07	0.00	0.21	0.29	−0.05	0.02	0.03	−0.40	−0.42	0.44	0.38	−0.55	**1.00**	−0.61	0.15	**0.85**	0.45	0.39	0.48
	Slope	0.16	0.61	−0.64	−0.67	−0.63	−0.60	0.36	0.54	0.39	0.35	**0.77**	0.32	−0.07	−0.17	0.68	−0.61	**1.00**	−0.42	**−0.91**	**−0.81**	**−0.73**	**−0.81**
	Aspect	−0.61	−0.32	0.02	0.19	0.49	−0.06	−0.03	−0.04	0.05	0.07	−0.38	−0.61	0.04	−0.04	−0.15	0.15	−0.42	**1.00**	0.35	−0.14	−0.25	−0.14
	SVF	−0.06	−0.41	0.54	0.50	0.46	0.50	−0.18	−0.46	−0.29	−0.25	**−0.77**	−0.41	0.18	0.28	**−0.72**	**0.85**	**−0.91**	0.35	**1.00**	**0.71**	0.63	**0.72**
	S_{in}	0.06	−0.60	0.69	0.68	0.50	0.68	−0.47	−0.61	−0.51	−0.48	−0.58	0.08	−0.07	0.02	−0.58	0.45	**−0.81**	−0.14	**0.71**	**1.00**	**0.99**	**1.00**
	$S_{in}^{(Winter)}$	0.08	−0.57	0.65	0.65	0.46	0.65	−0.46	−0.58	−0.51	−0.48	−0.50	0.16	−0.12	−0.05	−0.54	0.39	**−0.73**	−0.25	0.63	**0.99**	**1.00**	**0.99**
	$S_{in}^{(Summer)}$	0.07	−0.59	0.69	0.68	0.49	0.68	−0.45	−0.60	−0.52	−0.49	−0.58	0.08	−0.07	0.02	−0.61	0.48	**−0.81**	−0.14	**0.72**	**1.00**	**0.99**	**1.00**

https://doi.org/10.5194/tc-20-1001-2026

Data availability. The ground surface temperature data, hemispherical images, snow-, surface cover-, and vegetation surveys are available from https://doi.org/10.5281/zenodo.15470689 (Zweigel, 2025).

Author contributions. RBZ and SW conceptualized the study and collected the field data together with AD, TK and CW. RBZ led the formal analysis and investigation and wrote the initial draft with contributions from all co-authors. AD and SW administrated the project, and HL and SW acquired funding and contributed with supervision.

Competing interests. At least one of the (co-)authors is a member of the editorial board of *The Cryosphere*. The peer-review process was guided by an independent editor, and the authors also have no other competing interests to declare.

Disclaimer. Publisher's note: Copernicus Publications remains neutral with regard to jurisdictional claims made in the text, published maps, institutional affiliations, or any other geographical representation in this paper. The authors bear the ultimate responsibility for providing appropriate place names. Views expressed in the text are those of the authors and do not necessarily reflect the views of the publisher.

Acknowledgements. We thank the editor, Krystyna Kozioł, and two anonymous referees for taking the time to evaluate this manuscript. We also thank the National Agency for Meteorology and Environmental Monitoring of Mongolia for providing the meteorological data for Nalaikh.

Financial support. This research has been supported by the Research Council of Norway (Permafrost4Life (grant no. 301639), PRISM (grant no. 309625)) and the European Space Agency CCI+ Permafrost (grant no. 4000123681/18/I-NB).

Review statement. This paper was edited by Krystyna Kozioł and reviewed by Piotr Owczarek and one anonymous referee.

References

Angerer, J., Han, G., Fujisaki, I., and Havstad, K.: Climate Change and Ecosystems of Asia With Emphasis on Inner Mongolia and Mongolia, Rangelands, 30, 46–51, https://doi.org/0.2111/1551-501X(2008)30[46:CCAEOA]2.0.CO;2, 2008.

Bendavid, N. S., Alexander, H. D., Davydov, S. P., Kropp, H., Mack, M. C., Natali, S. M., Spawn-Lee, S. A., Zimov, N. S., and Loranty, M. M.: Shrubs Compensate for Tree Leaf Area Variation and Influence Vegetation Indices in Post-Fire Siberian Larch Forests, J. Geophys. Res.-Biogeo., 128, e2022JG007107, https://doi.org/10.1029/2022JG007107, 2023.

Beringer, J., Lynch, A. H., Chapin, F. S., Mack, M., and Bonan, G. B.: The Representation of Arctic Soils in the Land Surface Model: The Importance of Mosses, J. Climate, 14, 3324–3335, https://doi.org/10.1175/1520-0442(2001)014<3324:TROASI>2.0.CO;2, 2001.

Bonan, G.: Ecological Climatology: concepts and applications, 3rd edn., Cambridge University Press, https://doi.org/10.1017/CBO9781107339200, 2016.

Bonan, G. B. and Shugart, H. H.: Environmental Factors and Ecological Processes in Boreal Forests, Annu. Rev. Ecol. Syst., 20, 1–28, https://doi.org/10.1146/annurev.es.20.110189.000245, 1989.

Bréda, N. J. J.: Ground-based measurements of leaf area index: a review of methods, instruments and current controversies, J. Exp. Bot., 54, 2403–2417, https://doi.org/10.1093/jxb/erg263, 2003.

Chang, X., Jin, H., Zhang, Y., He, R., Luo, D., Wang, Y., Lü, L., and Zhang, Q.: Thermal Impacts of Boreal Forest Vegetation on Active Layer and Permafrost Soils in Northern da Xing'Anling (Hinggan) Mountains, Northeast China, Arct. Antarct. Alp. Res., 47, 267–279, https://doi.org/10.1657/aaar00c-14-016, 2015.

Chasmer, L., Quinton, W., Hopkinson, C., Petrone, R., and Whittington, P.: Vegetation Canopy and Radiation Controls on Permafrost Plateau Evolution within the Discontinuous Permafrost Zone, Northwest Territories, Canada, Permafr. Periglac. Process., 22, 199–213, https://doi.org/10.1002/ppp.724, 2011.

Chen, J. and Cihlar, J.: Quantifying the effect of canopy architecture on optical measurements of leaf area index using two gap size analysis methods, IEEE Trans. Geosci. Remote Sens., 33, 777–787, https://doi.org/10.1109/36.387593, 1995.

Chen, J., Black, T. A., and Adams, R. S.: Evaluation of hemispherical photography for determining plant area index and geometry of a forest stand, Agric. For. Meteorol., 56, 129–143, https://doi.org/10.1016/0168-1923(91)90108-3, 1991.

Dalai, S., Dambaravjaa, O., and Purevjav, G.: Water Challenges in Ulaanbaatar, Mongolia, in: Urban Drought: Emerging Water Challenges in Asia, edited by: Ray, B. and Shaw, R., Springer Singapore, Singapore, 347–361, https://doi.org/10.1007/978-981-10-8947-3_20, 2019.

Dashtseren, A., Ishikawa, M., Iijima, Y., and Jambaljav, Y.: Temperature regimes of the active layer and seasonally frozen ground under a forest-steppe mosaic, Mongolia, Permafr. Periglac. Process., 25, 295–306, https://doi.org/10.1002/ppp.1824, 2014.

Dozier, J. and Frew, J.: Rapid calculation of terrain parameters for radiation modeling from digital elevation data, IEEE T. Geosci. Remote, 28, 963–969, https://doi.org/10.1109/36.58986, 1990.

Dulamsuren, C., Hauck, M., Khishigjargal, M., Leuschner, H. H., and Leuschner, C.: Diverging climate trends in Mongolian taiga forests influence growth and regeneration of Larix sibirica, Oecologia, 163, 1091–1102, https://doi.org/10.1007/s00442-010-1689-y, 2010.

Esri: World Imagery [Web map], Scale not given, Esri World Imagery, https://www.arcgis.com/home/webmap/viewer.html?webmap=50c23e4987a44de4ab163e1baeab4a46. (last access: 9 January 2026), 8 September 2022.

Fedorov, A. N., Iwahana, G., Konstantinov, P. Y., Machimura, T., Argunov, R. N., Efremov, P. V., Lopez, L. M. C., and Takakai, F.: Variability of Permafrost and Landscape Conditions Following Clear Cutting of Larch Forest in

Central Yakutia, Permafr. Periglac. Process., 28, 331–338, https://doi.org/10.1002/ppp.1897, 2017.

Fernández-Giménez, M. E., Allington, G. R. H., Angerer, J., Reid, R. S., Jamsranjav, C., Ulambayar, T., Hondula, K., Baival, B., Batjav, B., Altanzul, T., and Baasandorj, Y.: Using an integrated social-ecological analysis to detect effects of household herding practices on indicators of rangeland resilience in Mongolia, Environ. Res. Lett., 13, 075010, https://doi.org/10.1088/1748-9326/aacf6f, 2018.

Fisher, J., Estop-Aragonés, C., Thierry, A., Charman, D. J., Wolfe, S. A., Hartley, I. P., Murton, J. B., Williams, M., and Phoenix, G. K.: The influence of vegetation and soil characteristics on active-layer thickness of permafrost soils in boreal forest, Glob. Change Biol., 22, 3127–3140, https://doi.org/10.1111/gcb.13248, 2016.

Ganbat, G. and Baik, J.-J.: Wintertime winds in and around the Ulaanbaatar metropolitan area in the presence of a temperature inversion, Asia-Pac, J. Atmospheric Sci., 52, 309–325, https://doi.org/10.1007/s13143-016-0007-y, 2016.

Gerelchuluun, B. and Ahn, J. B.: Air temperature distribution over Mongolia using dynamical downscaling and statistical correction, Int. J. Climatol., 34, 2464–2476, https://doi.org/10.1002/JOC.3853, 2014.

Glenn, E. P., Huete, A. R., Nagler, P. L., and Nelson, S. G.: Relationship Between Remotely-sensed Vegetation Indices, Canopy Attributes and Plant Physiological Processes: What Vegetation Indices Can and Cannot Tell Us About the Landscape, Sensors, 8, 2136–2160, https://doi.org/10.3390/s8042136, 2008.

Hartmann, D. L.: Global Physical Climatology, 2nd edn., Elsevier, 485 pp., ISBN-13 978-01232853-1, 2016.

Hersbach, H., Bell, B., Berrisford, P., Hirahara, S., Horányi, A., Muñoz-Sabater, J., Nicolas, J., Peubey, C., Radu, R., Schepers, D., Simmons, A., Soci, C., Abdalla, S., Abellan, X., Balsamo, G., Bechtold, P., Biavati, G., Bidlot, J., Bonavita, M., Chiara, G., Dahlgren, P., Dee, D., Diamantakis, M., Dragani, R., Flemming, J., Forbes, R., Fuentes, M., Geer, A., Haimberger, L., Healy, S., Hogan, R. J., Hólm, E., Janisková, M., Keeley, S., Laloyaux, P., Lopez, P., Lupu, C., Radnoti, G., Rosnay, P., Rozum, I., Vamborg, F., Villaume, S., and Thépaut, J.-N.: The ERA5 global reanalysis, Q. J. Roy. Meteor. Soc., 146, 1999–2049, https://doi.org/10.1002/qj.3803, 2020.

Hiemstra, C. A., Liston, G. E., and Reiners, W. A.: Snow Redistribution by Wind and Interactions with Vegetation at Upper Treeline in the Medicine Bow Mountains, Wyoming, U.S.A., Arct. Antarct. Alp. Res., 34, 262–273, https://doi.org/10.1080/15230430.2002.12003493, 2002.

Hong, S.-H., Lkhamjav, J., Jin, H.-G., and Baik, J.-J.: Spatiotemporal variations of 100 m wind in Mongolia and implications for wind energy resources, Int. J. Climatol., 43, 3433–3452, https://doi.org/10.1002/joc.8037, 2023.

Iijima, Y., Ishikawa, M., and Jambaljav, Y.: Hydrological cycle in relation to permafrost environment in forest-grassland ecotone in Mongolia, J. Jpn. Assoc. Hydrol. Sci., 42, 119–130, https://doi.org/10.4145/jahs.42.119, 2012.

Ishikawa, M., Sharkhuu, N., Zhang, Y., Kadota, T., and Ohata, T.: Ground thermal and moisture conditions at the southern boundary of discontinuous permafrost, Mongolia, Permafr. Periglac. Process., 16, 209–216, https://doi.org/10.1002/PPP.483, 2005.

Ishikawa, M., Jamvaljav, Y., Dashtseren, A., Sharkhuu, N., Davaa, G., Iijima, Y., Baatarbileg, N., and Yoshikawa, K.: Thermal states, responsiveness and degradation of marginal permafrost in Mongolia, Permafr. Periglac. Process., 29, 271–282, https://doi.org/10.1002/PPP.1990, 2018.

Iwahana, G., Machimura, T., Kobayashi, Y., Fedorov, A. N., Konstantinov, P. Y., and Fukuda, M.: Influence of forest clear-cutting on the thermal and hydrological regime of the active layer near Yakutsk, eastern Siberia, J. Geophys. Res.-Biogeo., 110, https://doi.org/10.1029/2005JG000039, 2005.

Jafarov, E. E., Marchenko, S. S., and Romanovsky, V. E.: Numerical modeling of permafrost dynamics in Alaska using a high spatial resolution dataset, The Cryosphere, 6, 613–624, https://doi.org/10.5194/tc-6-613-2012, 2012.

Janse, R. J., Hoekstra, T., Jager, K. J., Zoccali, C., Tripepi, G., Dekker, F. W., and van Diepen, M.: Conducting correlation analysis: important limitations and pitfalls, Clin. Kidney J., 14, 2332–2337, https://doi.org/10.1093/ckj/sfab085, 2021.

Jonas, T., Webster, C., Mazzotti, G., and Malle, J.: HPEval: A canopy shortwave radiation transmission model using high-resolution hemispherical images, Agric. For. Meteorol., 284, 107903, https://doi.org/10.1016/j.agrformet.2020.107903, 2020.

Karthe, D., Malsy, M., Kopp, S., Minderlein, S., and Hülsmann, L.: Assessing water availability and its drivers in the context of an integrated water resources management (IWRM): a case study from the Kharaa River Basin, Mongolia, GeoÖko, 34, 5–26, 2013.

Kasischke, E. S. and Johnstone, J. F.: Variation in postfire organic layer thickness in a black spruce forest complex in interior Alaska and its effects on soil temperature and moisture, Can. J. For. Res., 35, 2164–2177, https://doi.org/10.1139/x05-159, 2005.

Klinge, M., Dulamsuren, C., Erasmi, S., Karger, D. N., and Hauck, M.: Climate effects on vegetation vitality at the treeline of boreal forests of Mongolia, Biogeosciences, 15, 1319–1333, https://doi.org/10.5194/bg-15-1319-2018, 2018.

Klinge, M., Schneider, F., Dulamsuren, C., Arndt, K., Bayarsaikhan, U., and Sauer, D.: Interrelations between relief, vegetation, disturbances, and permafrost in the forest-steppe of central Mongolia, Earth Surf. Process. Landf., 46, 1766–1782, https://doi.org/10.1002/esp.5116, 2021.

Kopp, B., Minderlein, S., and Menzel, L.: Soil moisture dynamics in a mountainous headwater area in the discontinuous permafrost zone of northern Mongolia, Arct. Antarct. Alp. Res., 46, 459–470, https://doi.org/10.1657/1938-4246-46.2.459, 2014.

Koutantou, K., Mazzotti, G., Brunner, P., Webster, C., and Jonas, T.: Exploring snow distribution dynamics in steep forested slopes with UAV-borne LiDAR, Cold Reg. Sci. Technol., 200, 103587, https://doi.org/10.1016/j.coldregions.2022.103587, 2022.

Lang, A. R. G.: Simplified estimate of leaf area index from transmittance of the sun's beam, Agric. For. Meteorol., 41, 179–186, https://doi.org/10.1016/0168-1923(87)90078-5, 1987.

Lange, J., Kopp, B. J., Bents, M., and Menzel, L.: Tracing variability of run-off generation in mountainous permafrost of semi-arid north-eastern Mongolia, Hydrol. Process., 29, 1046–1055, https://doi.org/10.1002/HYP.10218, 2015.

Li, X., Jin, H.-J., Wang, H.-W., Marchenko, S. S., Shan, W., Luo, D.-L., He, R.-X., Spektor, V., Huang, Y.-D., Li, X.-Y., and Jia, N.: Influences of forest fires on the permafrost environment: A review, Spec. Top. Degrading Permafr. Its Impacts, 12, 48–65, https://doi.org/10.1016/j.accre.2021.01.001, 2021.

Liu, J., Li, L., Akerblom, M., Wang, T., Skidmore, A., Zhu, X., and Heurich, M.: Comparative Evaluation of Algorithms for Leaf Area Index Estimation from Digital Hemispherical Photography through Virtual Forests, Remote Sens., 13, https://doi.org/10.3390/rs13163325, 2021.

Lkhagvadorj, D., Hauck, M., Dulamsuren, Ch., and Tsogtbaatar, J.: Pastoral nomadism in the forest-steppe of the Mongolian Altai under a changing economy and a warming climate, J. Arid Environ., 88, 82–89, https://doi.org/10.1016/j.jaridenv.2012.07.019, 2013a.

Lkhagvadorj, D., Hauck, M., Dulamsuren, C., and Tsogtbaatar, J.: Twenty Years After Decollectivization: Mobile Livestock Husbandry and Its Ecological Impact in the Mongolian Forest-Steppe, Hum. Ecol., 41, 725–735, https://doi.org/10.1007/s10745-013-9599-3, 2013b.

Loranty, M. M., Davydov, S. P., Kropp, H., Alexander, H. D., Mack, M. C., Natali, S. M., and Zimov, N. S.: Vegetation Indices Do Not Capture Forest Cover Variation in Upland Siberian Larch Forests, Remote Sens., 10, https://doi.org/10.3390/rs10111686, 2018.

Lundberg, A. and Koivusalo, H.: Estimating winter evaporation in boreal forests with operational snow course data, Hydrol. Process., 17, 1479–1493, https://doi.org/10.1002/hyp.1179, 2003.

Mahat, V. and Tarboton, D. G.: Canopy radiation transmission for an energy balance snowmelt model, Water Resour. Res., 48, https://doi.org/10.1029/2011WR010438, 2012.

Maxim Integrated: DS1922L/DS1922T iButton Temperature Loggers with 8KB Datalog Memory Data Sheet (Rev. 13), Maxim Integrated, 2015.

NASA JPL: NASA Shuttle Radar Topography Mission (SRTM): Shuttle Radar Topography Mission (SRTM) Global 1 arc second, OpenTopography [data set], https://doi.org/10.5069/G9445JDF (last access: 9 January 2026), 2013.

Obu, J., Westermann, S., Bartsch, A., Berdnikov, N., Christiansen, H. H., Dashtseren, A., Delaloye, R., Elberling, B., Etzelmüller, B., Kholodov, A., Khomutov, A., Kääb, A., Leibman, M. O., Lewkowicz, A. G., Panda, S. K., Romanovsky, V., Way, R. G., Westergaard-Nielsen, A., Wu, T., Yamkhin, J., and Zou, D.: Northern Hemisphere permafrost map based on TTOP modelling for 2000–2016 at 1 km^2 scale, Earth-Sci. Rev., 193, 299–316, https://doi.org/10.1016/j.earscirev.2019.04.023, 2019.

Roy, D. and Zhang, H.: NASA Global Web-Enabled Landsat Data Monthly Global 30 m V031, Earth Data [data set], https://doi.org/10.5067/MEASURES/GWELD/GWELDMO.031, 2019.

Schleppi, P., Conedera, M., Sedivy, I., and Thimonier, A.: Correcting non-linearity and slope effects in the estimation of the leaf area index of forests from hemispherical photographs, Agric. For. Meteorol., 144, 236–242, https://doi.org/10.1016/j.agrformet.2007.02.004, 2007.

Schlütz, F., Dulamsuren, C., Wieckowska, M., Mühlenberg, M., and Hauck, M.: Late Holocene vegetation history suggests natural origin of steppes in the northern Mongolian mountain taiga, Palaeogeogr. Palaeoclimatol. Palaeoecol., 261, 203–217, https://doi.org/10.1016/j.palaeo.2007.12.012, 2008.

Schmidt, J. U., Etzelmüller, B., Schuler, T. V., Magnin, F., Boike, J., Langer, M., and Westermann, S.: Surface temperatures and their influence on the permafrost thermal regime in high-Arctic rock walls on Svalbard, The Cryosphere, 15, 2491–2509, https://doi.org/10.5194/tc-15-2491-2021, 2021.

Smith, M. and Riseborough, D. W.: Permafrost monitoring and detection of climate change, Permafr. Periglac. Process., 7, 301–309, https://doi.org/10.1002/(SICI)1099-1530(199610)7:4<301::AID-PPP231>3.0.CO;2-R, 1996.

Smith, M. and Riseborough, D. W.: Climate and the limits of permafrost: a zonal analysis, Permafr. Periglac. Process., 13, 1–15, https://doi.org/10.1002/ppp.410, 2002.

Stuenzi, S. M., Boike, J., Cable, W., Herzschuh, U., Kruse, S., Pestryakova, L. A., Schneider von Deimling, T., Westermann, S., Zakharov, E. S., and Langer, M.: Variability of the surface energy balance in permafrost-underlain boreal forest, Biogeosciences, 18, 343–365, https://doi.org/10.5194/bg-18-343-2021, 2021a.

Stuenzi, S. M., Boike, J., Gädeke, A., Herzschuh, U., Kruse, S., Pestryakova, L. A., Westermann, S., and Langer, M.: Sensitivity of ecosystem-protected permafrost under changing boreal forest structures, Environ. Res. Lett., 16, 084045, https://doi.org/10.1088/1748-9326/ac153d, 2021b.

Stuenzi, S. M., Kruse, S., Boike, J., Herzschuh, U., Oehme, A., Pestryakova, L. A., Westermann, S., and Langer, M.: Thermohydrological Impact of Forest Disturbances on Ecosystem-Protected Permafrost, J. Geophys. Res.-Biogeo., 127, e2021JG006630, https://doi.org/10.1029/2021JG006630, 2022.

Sturm, M., Holmgren, J., McFadden, J. P., Liston, G. E., Chapin, F. S., and Racine, C. H.: Snow–Shrub Interactions in Arctic Tundra: A Hypothesis with Climatic Implications, J. Climate, 14, 336–344, https://doi.org/10.1175/1520-0442(2001)014<0336:SSIIAT>2.0.CO;2, 2001.

Sugimoto, A., Yanagisawa, N., Naito, D., Fujita, N., and Maximov, T. C.: Importance of permafrost as a source of water for plants in east Siberian taiga, Ecol. Res., 17, 493–503, https://doi.org/10.1046/j.1440-1703.2002.00506.x, 2002.

Sumiya, E., Dorligjav, S., Purevtseren, M., Gombodorj, G., Byamba-Ochir, M., Dugerjav, O., Sugar, M., Batsuuri, B., and Tsegmid, B.: Climate Patterns Affecting Cold Season Air Pollution of Ulaanbaatar City, Mongolia, Climate, 11, https://doi.org/10.3390/cli11010004, 2023.

Temuujin, K., Dashtseren, A., Etzelmüller, B., Undrakhtsetseg, T., Aalstad, K., and Westermann, S.: Spatial variability of near-surface ground temperatures in a discontinuous permafrost area in Mongolia, Front. Earth Sci., 12, https://doi.org/10.3389/feart.2024.1456012, 2024.

Thimonier, A., Sedivy, I., and Schleppi, P.: Estimating leaf area index in different types of mature forest stands in Switzerland: a comparison of methods, Eur. J. For. Res., 129, 543–562, https://doi.org/10.1007/s10342-009-0353-8, 2010.

Tsogtbaatar, J.: Deforestation and reforestation needs in Mongolia, Restor. Res. Degraded For. Ecosyst., 201, 57–63, https://doi.org/10.1016/j.foreco.2004.06.011, 2004.

Undrakhbayar, E., Avirmed, D., Khurelbaatar, T., and Ariunbold, M.: Relationship between near ground surface temperature and land cover types of eastern lake Khuvsgul, Mong. J. Geogr. Geoecology, 61, 18–30, https://doi.org/10.5564/mjgg.v61i45.3343, 2024.

Walvoord, M. A. and Kurylyk, B. L.: Hydrologic Impacts of Thawing Permafrost-A Review, Vadose Zone J., 15, vzj2016.01.0010-

vzj2016.01.0010, https://doi.org/10.2136/vzj2016.01.0010, 2016.

Webster, C., Rutter, N., Zahner, F., and Jonas, T.: Modeling subcanopy incoming longwave radiation to seasonal snow using air and tree trunk temperatures, J. Geophys. Res.-Atmos., 121, 1220–1235, https://doi.org/10.1002/2015JD024099, 2015.

Westermann, S., Østby, T. I., Gisnås, K., Schuler, T. V., and Etzelmüller, B.: A ground temperature map of the North Atlantic permafrost region based on remote sensing and reanalysis data, The Cryosphere, 9, 1303–1319, https://doi.org/10.5194/tc-9-1303-2015, 2015.

Yi, S., Woo, M., and Arain, M. A.: Impacts of peat and vegetation on permafrost degradation under climate warming, Geophys. Res. Lett., 34, https://doi.org/10.1029/2007GL030550, 2007.

Yoshikawa, K., Bolton, W. R., Romanovsky, V. E., Fukuda, M., and Hinzman, L. D.: Impacts of wildfire on the permafrost in the boreal forests of Interior Alaska, J. Geophys. Res., 108, https://doi.org/10.1029/2001jd000438, 2002.

Zamba, B.: THIRD NATIONAL COMMUNICATION OF MONGOLIA, Ministry of Environment and Tourism, Mongolia, Ulaanbaatar, Mongolia, 2018.

Zhang, T.: Influence of the seasonal snow cover on the ground thermal regime: An overview, Rev. Geophys., 43, RG4002–RG4002, https://doi.org/10.1029/2004RG000157, 2005.

Zhang, T., Osterkamp, T. E., and Stamnes, K.: Effects of Climate on the Active Layer and Permafrost on the North Slope of Alaska, U.S.A., Permafr. Periglac. Process., 8, 45–67, https://doi.org/10.1002/(SICI)1099-1530(199701)8:1<45::AID-PPP240>3.0.CO;2-K, 1997.

Zhang, Y., Chen, J. M., and Miller, J. R.: Determining digital hemispherical photograph exposure for leaf area index estimation, Agric. For. Meteorol., 133, 166–181, https://doi.org/10.1016/j.agrformet.2005.09.009, 2005.

Zhao, Y.-Y., Li, Z.-T., Xu, T., and Lou, A.: Leaf litter decomposition characteristics and controlling factors across two contrasting forest types, J. Plant Ecol., 15, 1285–1301, https://doi.org/10.1093/jpe/rtac073, 2022.

Zweigel, R. B.: Research data for egusphere-2025-2366, Zenodo [data set], https://doi.org/10.5281/zenodo.15470689, 2025.

Zweigel, R. B., Westermann, S., Nitzbon, J., Langer, M., Boike, J., Etzelmüller, B., and Vikhamar Schuler, T.: Simulating Snow Redistribution and its Effect on Ground Surface Temperature at a High-Arctic Site on Svalbard, J. Geophys. Res.-Earth Surf., 126, e2020JF005673, https://doi.org/10.1029/2020JF005673, 2021.

Zweigel, R. B., Dashtseren, A., Temuujin, K., Aalstad, K., Webster, C., Stuenzi, S. M., Aas, K. S., Lee, H., and Westermann, S.: Simulating the Thermal Regime and Surface Energy Balance of a Permafrost-Underlain Forest in Mongolia, J. Geophys. Res.-Earth Surf., 129, e2023JF007609, https://doi.org/10.1029/2023JF007609, 2024a.

Zweigel, R. B., Dashtseren, A., Temuujin, K., Sharkhuu, A., Webster, C., Lee, H., and Westermann, S.: Impact of livestock activity on near-surface ground temperatures in central Mongolian grasslands, Biogeosciences, 21, 5059–5077, https://doi.org/10.5194/bg-21-5059-2024, 2024b.